

Universität Stuttgart

**Institut für Photovoltaik  
Institute for Photovoltaics**



**Jahresbericht  
*Annual Report***

**2015  
2016**



## Inhaltsverzeichnis Table of Contents

<b>Vorwort</b> <b>Preface</b>	<b>3</b>
<b>Arbeitsgruppen</b> <b>Research Groups</b>	<b>4</b>
<b>Wissenschaftliche Beiträge</b> <b>Scientific Contributions</b>	<b>15</b>
<b>Publikationen</b> <b>Publications</b>	<b>54</b>
<b>Lehrveranstaltungen</b> <b>Lectures</b>	<b>59</b>
<b>Abschlüsse</b> <b>Degrees</b>	<b>67</b>
<b>Was sonst noch war</b> <b>Beyond Science</b>	<b>79</b>
<b>Mitarbeiterliste</b> <b>Staff Members</b>	<b>86</b>
<b>Gäste &amp; ausländische Stipendiaten</b> <b>Guests</b>	<b>89</b>
<b>Lageplan</b> <b>Location Map</b>	<b>90</b>

# Institutsleitung und Verwaltung

## Head of the Institute and Administration

(Leitung / Head: Jürgen H. Werner)



Jürgen H. Werner



Irmy Kerschbaum



Freymut Hilscher



Sabine Ost

**Liebe Freunde des *ipv*,**

nach den schwierigen Jahren 2013/14 geht es dem *ipv* inzwischen wieder richtig gut: Im Jahr 2016 haben wir so viele Drittmittel wie nie zuvor für unsere Photovoltaik-, Lasertechnik- und Medizintechnikforschung eingeworben. Hinzu kommt, dass der neu berufene Professor Peter Birke, der seit Anfang 2015 die neue Forschungsgruppe „Elektrische Energiespeichersysteme“ leitet, ebenfalls gut vorankommt beim Einwerben von Forschungsmitteln und Aufbau seiner Labore. Seit einiger Zeit ist es deshalb nicht nur möglich, dass wir höchsteffiziente Solarzellen, sondern auch Batteriezellen herstellen. Auch der Umbau des Reinraums verbessert unsere technischen Möglichkeiten und Arbeitsbedingungen. Aus diesen Gründen und wegen des großen Engagements und der Begeisterung unserer Mitarbeiter/innen blicken wir optimistisch in die Zukunft.

---

**Dear friends of the *ipv*,**

After the difficult years 2013/14, the *ipv* is doing quite well again: In the year 2016 we raised more money for our research in the fields of photovoltaics, laser processing, and medical technologies than ever before. In addition, Professor Peter Birke, the new head of the new research group „Electrical Energy Storage Systems“ proceeds very well with raising money as well as with establishing his lab. Therefore, we are now not only able to fabricate highly efficient solar cells, but also battery cells. The retrofitting of the cleanroom improves our technical abilities and working conditions even further. For these reasons, as well as due to the enthusiasm of all members of the institute, I am confident that the *ipv* will bloom in the coming years.

Stuttgart, Juli/July 2017

*Jürgen H. Werner*

# Industrielle Solarzellen Industrial Solar Cells

(Gruppenleiterin / Group Leader: Renate Zapf-Gottwick)



Renate Zapf-Gottwick

Osama Tobail



Kai Carstens

Erik Hoffmann



Simon Huber

Sabrina Lang



Jessica Nover

Sabine Schreiber

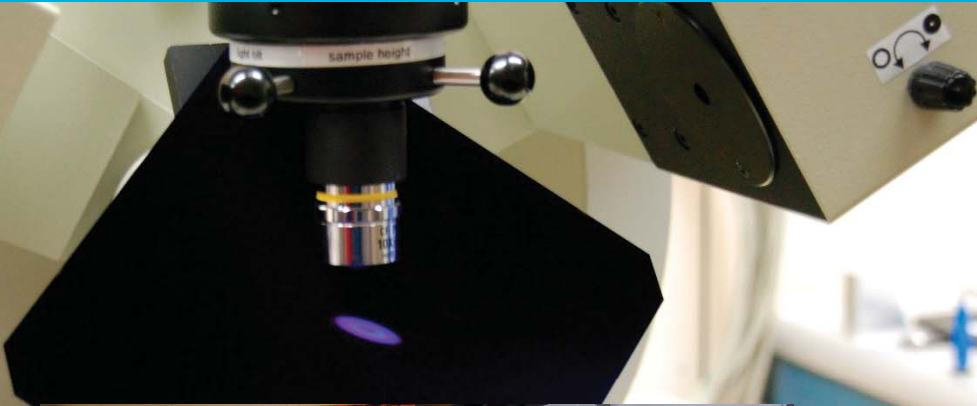
Die Gruppe „Industrielle Solarzellen“ erforscht und entwickelt neue und bestehende industriennahe Prozesse. Gemeinsam mit den *ipv*-Gruppen „Laserprozesse“ und „Halbleitertechnologie“ arbeiten wir an hocheffizienten Rückseitenkontakt-Solarzellen, die durch Laserprozesse schnell und kostengünstig produziert werden können. Den Wirkungsgrad von 23,3% auf Laborgröße von 4 cm<sup>2</sup> skalieren wir derzeit auf eine industriell relevante Fläche. Im Projekt „InES“ bauen wir zusammen mit den Baden-Württembergischen Forschungsinstituten IPA, ISC und ISE ein Technikum 4.0 auf. Im *ipv*-Teil optimieren wir den Siebdruck von Feinlinien-Kontakten auf Solarzellen und entwickeln eine Maschine für industrielle Laserprozesse. In einem weiteren Projekt streben wir nach einer „grüneren“ Photovoltaik und untersuchen, ob und wie Schadstoffe wie Cadmium und Blei aus defekten Photovoltaik-Modulen unterschiedlicher Technologien austreten.

---

Our group “Industrial Solar Cells” is engaged in research activities for higher efficiencies and lower production costs of solar cells in industry-oriented processes. Together with the *ipv*-groups “Laser Processing” and “Semiconductor Technology”, we develop high efficiency back contact solar cells. Laser processes reduce production costs and process time. We are scaling up the efficiency of 23.3% from a cell size of 4 cm<sup>2</sup> to an industrially relevant size. In the project “InES”, we cooperate with the research institutes IPA, ISC and ISE to set up an industry 4.0 technical center. The *ipv*'s part is the fine-line screen printing of the front side metallization and the development of an industrially feasible laser tool for doping. Another project aims at “greener” photovoltaics: we are studying the release of hazardous substances, like cadmium and lead, out of defective modules.

# Halbleitertechnologie Semiconductor Technology

(Gruppenleiterin / Group Leader: Birgitt Winter)



Birgitt Winter



Leo Bauer



Anton Riß



Lydia Beisel



Brigitte Lutz



Hendrik  
Moldenhauer

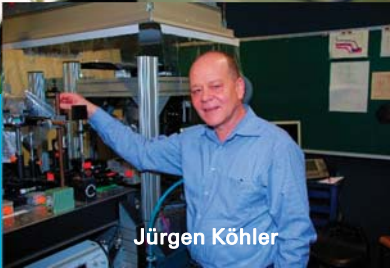
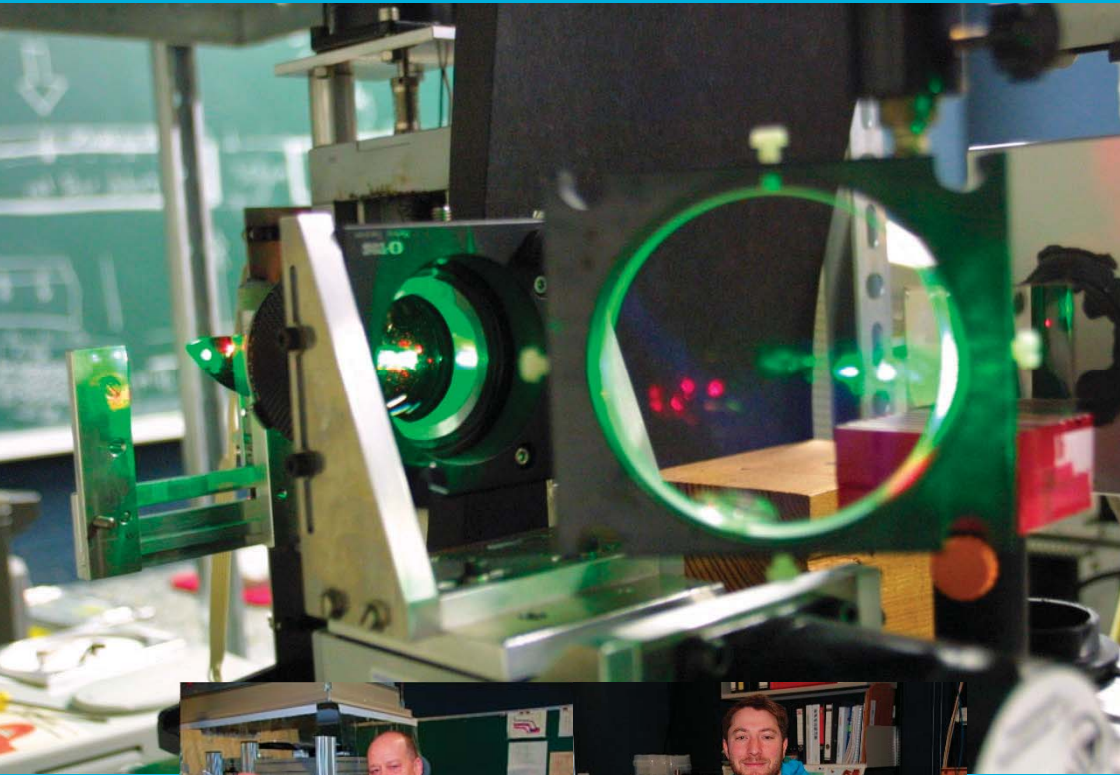
Die Gruppe „Halbleitertechnologie“ setzt sich aus den technischen Mitarbeiterinnen und Mitarbeitern des gesamten Instituts zusammen. Damit sind verschiedene Aufgabenstellungen zur Absicherung der Institutsinfrastruktur zusammengefasst. Die interdisziplinäre Vernetzung im technischen Bereich ermöglicht eine gute Koordinierung aller anfallenden Arbeiten. Im Jahr 2016 unterbrach die Erneuerung des Lüftungssystems im Reinraum die routinemäßige Durchführung von Prozessschritten wie Oxidationen, Diffusionen, Plasmadepositionen, nasschemisches Reinigen und Ätzen, Lithographie, Metallisierung, Laserdotieren und vieles andere. Deshalb standen am Ende des Jahres die Wiederinbetriebnahme aller Anlagen und das Validieren aller Prozesse im Vordergrund.

---

The group “Semiconductor Technology” includes all technical assistants and engineers of the institute. By joining forces, we are able to secure the entire infrastructure of the institute. The interdisciplinary composition of the technical team permits optimum coordination of all tasks. Last year, our regular operation of processes, such as oxidation, diffusion, plasma enhanced deposition, wet chemical cleaning and etching, lithography, metallization, laser doping, etc. was interrupted by the replacement of the ventilation system in the cleanroom. At the end of the year, our focus was therefore put on restarting all systems and validating all processes.

# Laserprozesse Laser Processing

(Gruppenleiter / Group Leader: Jürgen Köhler)



Jürgen Köhler



Morris Dahlinger



Mohamed Hassan



Patrick Lill

Die Gruppe „Laserprozesse“ entwickelt neue Technologien zum Laserprozessieren von Materialien für die Elektrotechnik. Neben dem Laser-Prozessieren kristalliner Silizium-Scheiben für Solarzellen und Halbleiterbauelemente, bildet die Herstellung poröser Anoden aus Silizium für Lithium-Ionen Batterien einen weiteren Schwerpunkt. Im Vordergrund unserer Arbeiten stehen die Weiterentwicklung unseres Laserdotier-Prozesses für rückseitenkontaktierte Solarzellen, sowie die Ablation dielektrischer Schichten. Weiterhin untersuchen wir das Dotieren und Aktivieren von Dotieratomen in einkristallinem Germanium für Halbleiterbauelemente sowie das Laser-Porosieren gesputterter Silizium-Schichten. In enger Zusammenarbeit mit den Gruppen „Industrielle Solarzellen“ und „Halbleitertechnologie“ am *ipv* optimieren wir unsere Laserprozesse zur Herstellung hocheffizienter, rückseitenkontaktierter Solarzellen mit Wirkungsgraden über 23%.

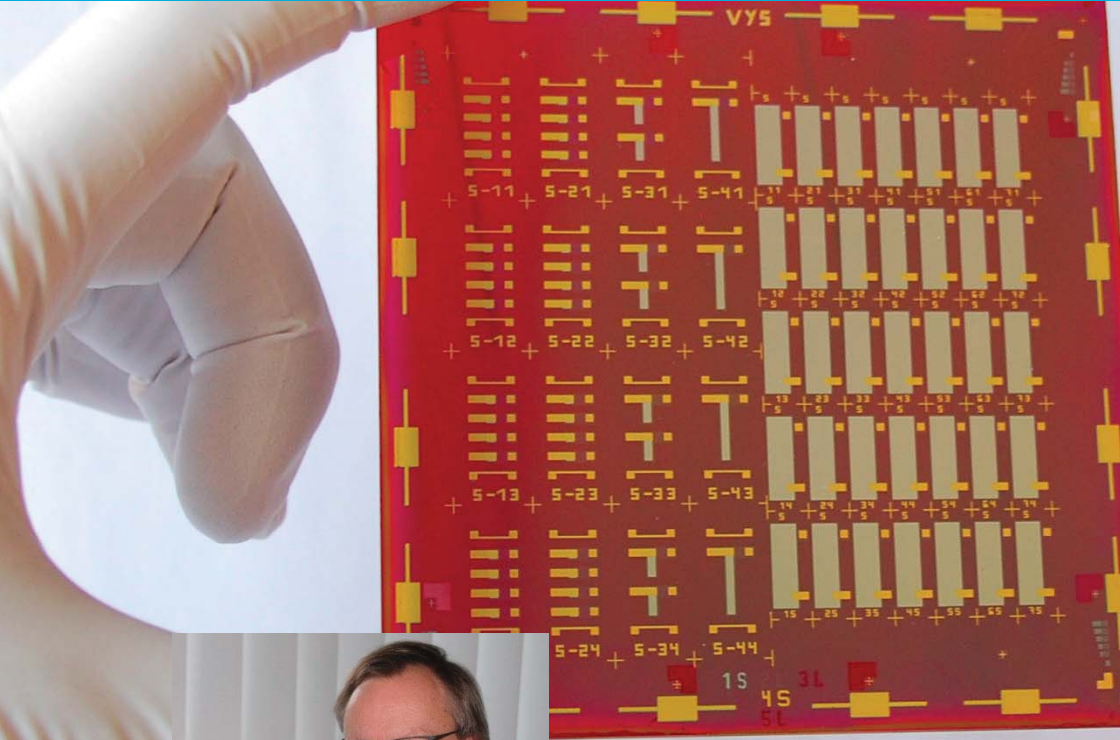
---

The “Laser Processing” group explores new technologies for laser processing of materials for electrical engineering applications. Porous anodes for lithium ion batteries are a new focus of our research, in addition to laser processing of crystalline silicon wafers for solar cells and semiconductor components. The main emphasis of our research lies on pulsed laser doping for high-efficiency back-contact solar cells, and the ablation of dielectric layers. Furthermore, we analyze the doping and dopant-atom activation of mono-crystalline germanium for semiconductor elements, as well as laser porosification of sputtered silicon layers. A close collaboration with the research groups “Industrial Solar Cells” and “Semiconductor Technology” at *ipv* optimizes our laser processes for the fabrication of high-efficiency back-contact solar cells with efficiencies above 23%.

# Sensorik

## Sensor Technology

(Gruppenleiter / Group Leader: Markus Schubert)



Markus Schubert



Timo Kropp



Christian Samann

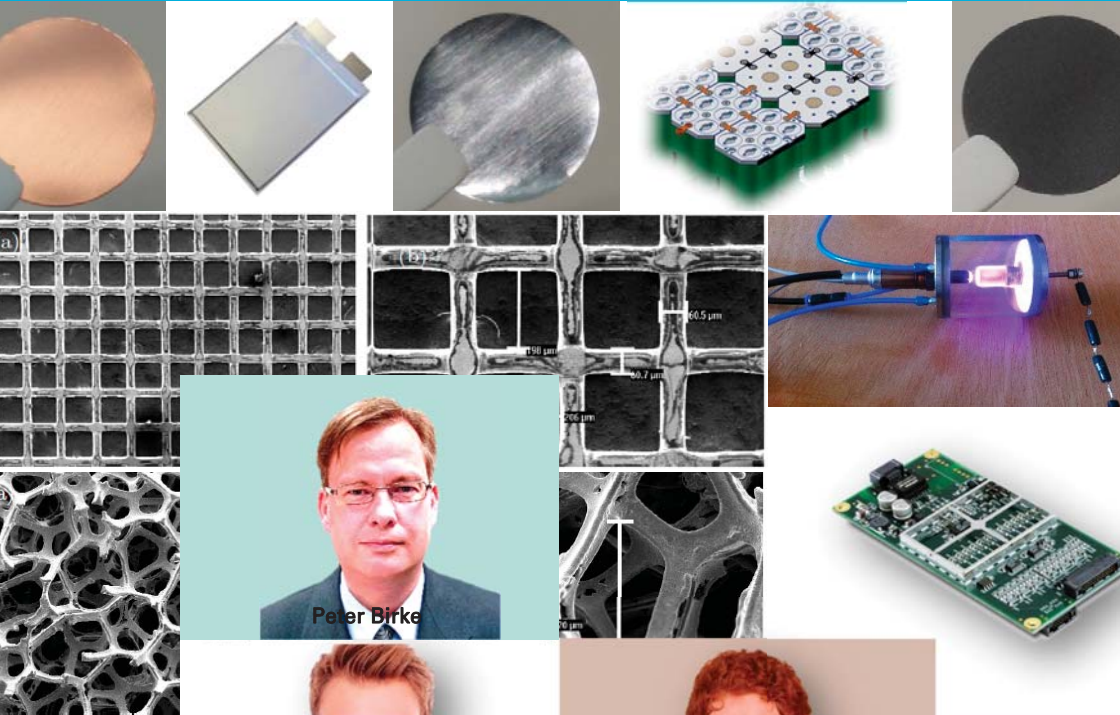
Die Arbeitsgruppe „Sensorik“ entwickelt Mess- und Modellierungsmethoden für Photovoltaikmodule und Solarparks, um deren aktuellen Zustand zu ermitteln und zukünftige Erträge abzuschätzen. Im Vorhaben PARK arbeiten wir dazu eng mit dem Solarzentrum Stuttgart zusammen. Hochempfindliche Dünnschichtphotodioden dienen im EU-Verbund NANODEM der kontinuierlichen Überwachung der Medikamentierung von Patienten nach Organtransplantationen. Unsere Begleitung und Auswertung des Praxistests eines elektrischen Quarterspeichers im Landesprojekt STROMBANK ist inzwischen abgeschlossen und die Weiterentwicklung poröser Si-Anoden für Lithium-Ionen-Batterien liefert vielversprechende Ergebnisse.

---

The "Sensor Technology" group at *ipv* develops methods for the characterization and modelling of photovoltaic modules and solar power plants in order to monitor their condition and to forecast their future energy yield. In the research project called PARK, we cooperate closely with the Solarzentrum Stuttgart. In the EU project NANODEM, high-sensitivity thin film photodiodes enable continuous monitoring of the immunosuppressant levels of patients after organ transplantation. Data acquisition and evaluation of the operation of a Li- ion battery container, called STROMBANK, i.e. Electricity Bank, has been finished. The development of porous Si anodes for Li-ion batteries shows promising results.

# Elektrische Energiespeichersysteme Electrical Energy Storage Systems

(Gruppenleiter / Group Leader: Peter Birke)



Peter Birke



Christoph Bolsinger



Alexander Schmid



Jan Singer



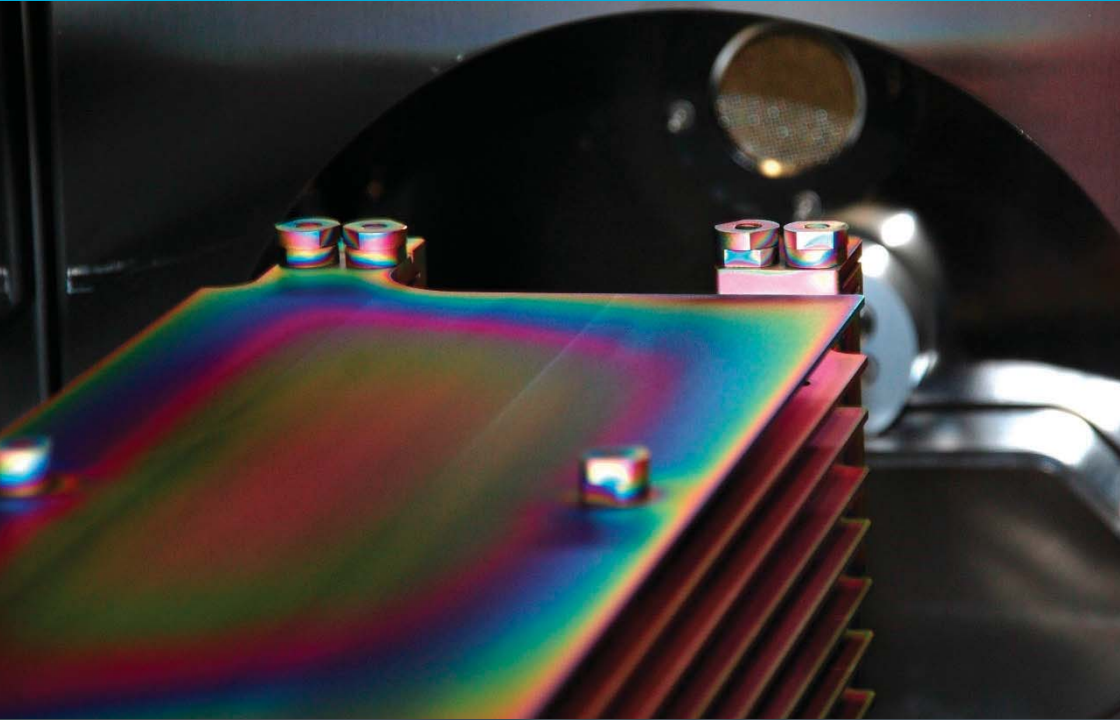
Friedrich Speckmann

Elektrische Energiespeichersysteme (EES) umfassen ein sehr weites Feld, denn darunter fallen im Prinzip alle Systeme, die elektrische Energie bidirektional in eine andere Energieform umwandeln können. Die Gruppe EES fokussiert sich bei der Zelle auf Lithium-basierte galvanische Elemente mit den Schwerpunkten feste Ionenleiter, Phasengrenzen und Strukturierung metallischer Li-Anoden. Systemseitig (Batterie) stehen Energiedichteerhöhung, elektrisches und thermisches Management sowie Batteriemodelle im Vordergrund der Forschung. Der Bereich Power to X (X=gas, liquid, solid) deckt Speicher ab, die als Batterie mit einer einmaligen Aufladung und anschließender Lagerung der Anode verstanden werden können. Die Lagerzeit ist beliebig lange, und die Anode kann danach in einer galvanischen Zelle wieder elektrische Energie liefern. Immer da, wo konventionelle Batterien an Kostengrenzen stoßen, können solche Systeme eine entscheidende Lücke füllen.

Electrical Energy Storage Systems (EES) cover a wide field of applications since they are systems able to convert electrical energy bidirectionally into another form of energy. On cell level, the group EES focusses on Lithium-based galvanic elements with research on solid ion conductors, phase boundaries and structures for metallic Li-anodes. On system level (battery), the focus of research is on energy density enhancement, electrical and thermal battery management and involved battery models. The field of power to X (X=gas, liquid, solid) covers energy storage systems, which are basically a reserve battery with a single charge step. The anodes can be separated, stored for an arbitrary time and they provide energy when reassembled in a galvanic cell afterwards. These systems can replace large cost-intensive batteries.



## Wissenschaftliche Beiträge Scientific Contributions



## Publikationen | Publications

## 22.0 % Efficient 5" Back Contact Solar Cells

Erik Hoffmann

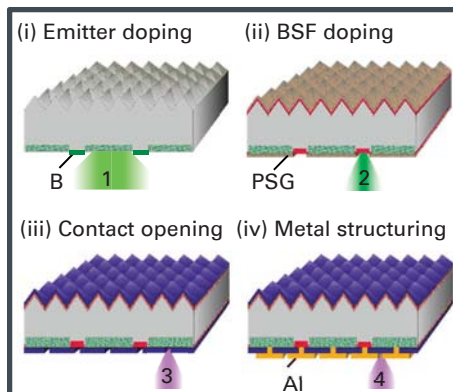
In collaboration with: Kai Carstens,  
and Morris Dahlinger

Crystalline silicon solar cells with interdigitated back contacts (IBC) currently yield a maximum efficiency  $\eta = 26.33\%$  [1]. The usually utilized processing sequence for IBC solar cells, however, requires expensive and time consuming masking steps. The *ipv* developed a fast, versatile and less expensive process for IBC solar cells, implementing four laser irradiation steps for (i) emitter and (ii) back surface field doping, (iii) local contact opening and (iv) metallization structuring. The laser steps avoid lithographic masking, but still allow fine patterning with a spatial accuracy  $d = \pm 45 \mu\text{m}$ , yielding  $\eta = 23.2\%$  on a cell area  $A = 4 \text{ cm}^2$  [2], and  $\eta = 22.0\%$  on  $A = 156 \text{ cm}^2$ .

Scaling the cell concept from  $A = 4 \text{ cm}^2$  to an industrial relevant 6 inch solar cell with  $A = 239 \text{ cm}^2$  requires homogeneous doping and passivation across the whole area and several busbars on the rear cell area. The silicon under each busbar needs to be doped according to the busbars polarity in order to prevent possible short circuits.

Figure 1 shows the four laser irradiation steps: (i) emitter doping from a sputtered boron precursor layer, (ii) backsur-

**Figure 1:** Laser irradiation steps of the *ipv* IBC solar cell process: (i) emitter doping from a boron (B) precursor layer, (ii) back surface field doping from phosphorous silicate glass, (iii) contact opening by ablation of the dielectric layer and (iv) structuring of the aluminum (Al) layer. All laser steps are homogenous across the cell area  $A = 156 \text{ cm}^2$  and locally defined with a spatial accuracy of  $d = \pm 45 \mu\text{m}$ .



face field doping from phosphorous silicate glass, (iii) ablation of the passivating layer and (iv) structuring of the evaporated aluminum layer into contact fingers. The 156 cm<sup>2</sup> sized cells are processed on standard 6 inch n-type Czochralski silicon wafers and finally cut to 156 cm<sup>2</sup> by laser scribing. We use three busbars of each polarity to interconnect the contact fingers. Tapering the busbars minimizes the required doping under the busbars, enhancing the solar cell efficiency by increasing both short circuit current density  $J_{sc}$  and fill factor  $FF$  due to reduced electrical shading and series resistance. Table 1 presents the current density/voltage ( $J/V$ )-parameters of the best cell with an area  $A = 4$  cm<sup>2</sup> and of the best cell with  $A = 156$  cm<sup>2</sup>. Both  $J_{sc}$  and  $FF$  of the larger cell are lower due the busbars being placed on the active cell area. The lower open circuit voltage  $V_{oc}$  results from laser cutting of the 6 inch wafer, which induces defects and additionally results in an unpassivated edge. Nevertheless the efficiency reaches  $\eta = 22.0\%$ , which proves the accuracy of the laser processes and the homogeneity of both, passivation and doping.

**Table 1:** Solar cell results of record solar cells sized  $A = 4$  cm<sup>2</sup> and  $A = 156$  cm<sup>2</sup>.

Area $A$ [cm <sup>2</sup> ]	$J_{sc}$ [mA/cm <sup>2</sup> ]	$V_{oc}$ [mV]	$FF$ [%]	$\eta$ [%]
4	41.3	682	82.5	23.2
156	40.6	672	80.3	22.0

The first scaling step of the  $ip\nu$  laser IBC solar cell from an area  $A = 4$  cm<sup>2</sup> to  $A = 156$  cm<sup>2</sup> shows that the four laser processes are homogenous and spatially accurate on the larger area. Next, we will scale up further to 6 inch solar cells. Additionally, we will implement a double layer metallization, which will increase  $J_{sc}$  and  $FF$  for efficiencies  $\eta > 22.0\%$ .

**References:**

[1] World’s Highest Conversion Efficiency of 26.33% Achieved in Crystalline Silicon Solar Cell, <http://www.nedo.go.jp> (2016)  
 [2] M. Dahlinger, K. Carstens, E. Hoffmann, R. Zapf-Gottwick, and J.H. Werner, Prog. Photovolt. **25**, 192 (2016).

# Laser-Induced Capillary Waves in Liquid Silicon

Jürgen Köhler

In collaboration with: Mohamed Hassan

During laser doping a pulsed laser melts the surface of a silicon wafer. Our patented defect free laser doping process uses a line-focused laser beam. Each laser pulse melts the silicon on an area about 7  $\mu\text{m}$  wide and 0.8 mm long.

In contrast to most other materials, liquid silicon has a density significantly higher than solid silicon at room temperature, similar to the densities of water and ice. This density anomaly leads to a strongly curved surface of the liquefied silicon when the melt reaches its maximum depth of about 500 nm.

Figure 1a shows the simulated surface of liquid silicon, molten by a 50 ns long laser pulse, if the liquid silicon is assumed not to move. The strong curvature of the liquid silicon surface, together with the surface tension, leads to the formation of a so-called capillary surface wave, travelling through the liquid silicon until it freezes during re-solidification. The result is a periodically textured surface on a laser processed silicon wafer.

The following three differential equations describe the temporal and spatial development of capillary waves [1]:

$$\rho \frac{\partial \Phi}{\partial t} = \alpha \frac{\partial^2 \zeta}{\partial x^2}, \quad \left\{ \frac{\partial^2}{\partial x^2} + \frac{\partial^2}{\partial z^2} \right\} \Phi = 0, \quad \frac{\partial \zeta}{\partial t} = \frac{\partial \Phi}{\partial z}. \quad (1)$$

Here,  $\Phi$  is the velocity potential, with  $v_{x,z} = \partial \Phi / \partial x, z$  being the velocity of the liquid silicon in x- / z-direction (parallel / perpendicular to the wafer surface),  $\rho$  is the density of liquid silicon,  $\alpha$  is the surface tension, and  $\zeta$  denotes the location of the surface of the liquid silicon.

Figure 1b shows the remaining textured surface of a silicon wafer after irradiation with a single laser pulse as the result of a numerical solution of equations (1).

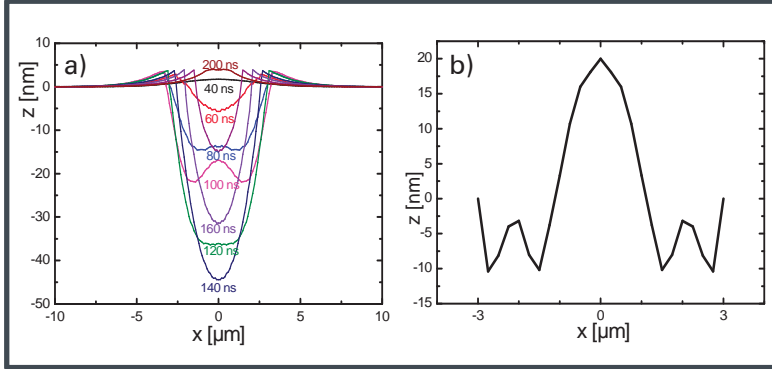


**Figure 1:** Liquid silicon has a significantly higher density than solid silicon at room temperature. This density anomaly leads to a curved surface of the liquefied silicon during irradiation with a laser pulse. The surface tension of liquid silicon then induces a capillary wave, which results in a textured surface after solidification. a) Simulated surface of liquid silicon for different times after the onset of a 50 ns laser pulse, if the liquid silicon is assumed not to move. b) Simulated frozen capillary wave on the surface of a silicon wafer.

So far, our numerical simulation of capillary surface waves does not account for the strong inertial forces resulting from the collapsing and expanding volume elements during liquefaction and re-solidification. Nevertheless, the results qualitatively agree with experimental results presented by Mohamed Hassan in his contribution “*Laser Processed Refraction Gratings for Improved Light Trapping in Solar Cells*” in this annual report.

**Reference:**

[1] L.D. Landau and E.M. Lifshitz. *Course of Theoretical Physics, Volume 6, Fluid Mechanics* (Pergamon Press Ltd., 1959), p. 237 - 241.

## **Porous Silicon Thin Film Anodes for Lithium Ion Batteries**

**Christian Sämman**

In collaboration with: Jürgen Köhler,  
Mario Wachtler (ZSW Ulm), Peter Birke,  
Markus Schubert, and Jürgen Werner

Extending the range of electric vehicles with equal weight requires further improvement of the specific energy of their batteries. Thus, research on new materials for batteries aims at increasing the specific capacity for portable applications.

One promising approach towards this end replaces the active material graphite of the negative electrode (anode) in conventional lithium ion batteries with silicon. Silicon has the highest known specific capacity  $C_{\text{Si}} = 1856 \text{ mAh/g}$  ( $\text{Li}_{15}\text{Si}_4$ ) for lithium, often erroneously reported as  $C_{\text{Si}} = 3579 \text{ mAh/g}$  by neglecting the Li mass. Hence, Si theoretically promises a fivefold capacity when compared with the specific capacity of graphite  $C_{\text{C}} = 339 \text{ mAh/g}$ .

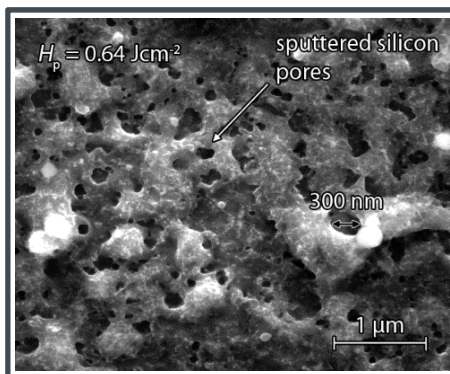
Silicon, unfortunately, expands up to 270% in volume during lithiation. This volume expansion causes mechanical damage of silicon during lithiation and delithiation by cracking or fracturing. The damage occurs especially during the first cycle, and often results in the loss of electrical contact to the current collector. Therefore, to prevent capacity fading during lithiation/delithiation, the microscopic morphology of silicon must change to accommodate such volume changes. Porous silicon, for example, meets these requirements. By allocating space for the expansion, pores in Si improve its ability to non-destructively change its volume. The pores reduce the induced stress and mechanical load, thus enabling a more stable capacity retention.

For forming porous silicon, we first deposit several 100 nm thick amorphous Si layers on metal foil current collectors by radio frequency sputtering.

Sputtering results in an incorporation of argon into the sputtered films, that we use as porosification source [1]. A pulsed laser beam in shape of a line and a wavelength  $\lambda = 532$  nm locally irradiates the Si thin films. The pulsed laser beam is scanned over the surface of the film. Strong absorption of the green laser radiation heats the silicon beyond the melting point. As soon as silicon undergoes the phase change from solid to liquid, incorporated gas atoms merge to gas bubbles. Further increase of the temperature during the laser pulse induces thermal expansion of the gas bubbles. Finally, they reach the surface and leave the film. After the laser pulse of  $100 \text{ ns} \leq \tau_p \leq 250 \text{ ns}$  duration, fast cooling and solidification of silicon creates the porous structured and laser crystallized thin film silicon.

Figure 1 shows a scanning electron microscopy image of Ar-sputtered  $d_{\text{Si}} = 200$  nm thick silicon on a steel foil substrate after laser irradiation.

**Figure 1:** Scanning electron microscopy image of porous silicon on stainless steel foil substrate after treatment by laser pulse energy density  $H_p = 0.64 \text{ Jcm}^{-2}$  and pulse duration  $\tau_p = 220 \text{ ns}$ . The created pores stabilize silicon during volume expansion due to lithiation/delithiation.



Such porous silicon films as negative electrodes show an improved cyclic stability compared to Si anodes without any laser treatment. Thus, the porosity of silicon increases the mechanical stability for the high volume changes. We achieve a stable cycling for more than 500 cycles. Further research pursues the porosification of thicker silicon films and optimized porosity for improved cycling stability.

#### References:

- [1] C. Sämann, J.R. Köhler, M. Dahlinger, M.B. Schubert, and J.H. Werner, *Materials* **9**, 509 (2016).

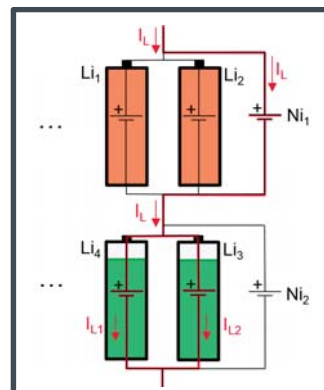
# Electrochemical Balancing of Lithium-Ion Cells

Alexander Schmid

In collaboration with: Kai Peter Birke, Ludwig Ehringer,  
and Ioannis Lambidis

Balancing of serially connected electrochemical cells is crucial. Imbalanced states of charge of electrochemical cells lead to lower storage capabilities in comparison to a system consisting of homogeneous electrochemical cells [1]. This study presents a new, cost-effective way to balance lithium-ion cells. The idea is to bypass charged lithium iron phosphate (LFP) or lithium titanate (LTO) cells by connecting them in parallel to nickel-based cells, which have different inherent electrochemical behavior. For this method, called *electrochemical balancing*, three major advantages arise: First, in the case of imbalanced states, electrochemical balancing does not only transform the energy into heat such as dissipative balancing methods, but also stores the energy needed for balancing in nickel-based cells by electrochemical reaction. Second, there is no need for additional active electrical components and complex balancing strategies [2]. Third, the safe system: the lithium-ion cells can not be overcharged due to the nickel-based cells' reversible gassing at moderate charging rates.

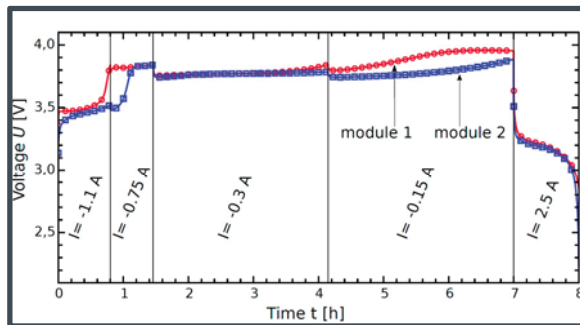
**Figure 1:** Electrochemical balancing of two serially connected modules. A module consists of two lithium-ion cells and one nickel-based cell. The lithium-ion cells of the upper module (module 1) are already fully charged. In contrast, the lithium-ion cells of the lower module (module 2) are partially charged.



The results show that balancing of lithium-ion cells is technically feasible for the following combinations only by connecting them in parallel with nickel-based cells: one LFP cell with 2 nickel zinc (NiZn) cells as well as 1 LTO cell connected in parallel with 2 nickel metal-hydride cells. The cyclization of both configurations indicated whole usability of the lithium-ion cells' capacity. In addition, the investigated lithium-ion cells do not suffer any overvoltage at moderate currents during charging. However, the nickel-based cells limit in particular the applicable c-rate during discharge. Therefore, nickel-based cells with high power characteristics are necessary for electrochemical balancing.

Figure 2 shows a further investigation with 2 serially connected modules, each module consisting of 1 LFP and 2 NiZn cells, which demonstrates the proof-of-concept of this balancing method. The initial charge imbalance between several LFP cells can be balanced due to reversible gassing of the used NiZn cells.

**Figure 2:** Balancing of 2 modules at different constant currents for one cycle. The charge imbalance of 100 mAh can be eliminated.



A cost-effective battery with advantages of both cell chemistries, robust lithium-ion cells with a high durability and high power nickel-based cells allows a new balancing method. In future, a charger with an optimized charge procedure could make a cell voltage measurement obsolete.

### References:

- [1] J. Cao, N. Schofield, and A. Emadi, in *Proc. 2006 IEEE Veh. Pow. and Propuls. Conf.* (Harbin, China, Sept. 2006)
- [2] G. Piatowicz, A. Marongiu, J. Drillkens, P. Sinhuber, and D.U. Sauer, *J. Power Sources* **296**, 365-376 (2015)

# Long Term Leaching of Photovoltaic Modules

Jessica Nover

In collaboration with: Renate Zapf-Gottwick,  
Carolin Feifel<sup>1</sup>, Michael Koch<sup>1</sup>, and Jürgen Werner

<sup>1</sup>Institute for Sanitary Engineering, Water Quality, and Solid Waste  
Management, University of Stuttgart, Germany

Many different elution tests for waste characterization exist worldwide to quantify leached elements out of different wastes and to classify them into risk groups. All these tests have different requirements regarding sample size, leaching solution and treatment method. One parameter, which is common to all tests, is a test duration of only 18 to 48 hours. Therefore, the tests have to apply conditions (e.g. orbital shaking or end-over-end agitation), which simulate accelerated aging.

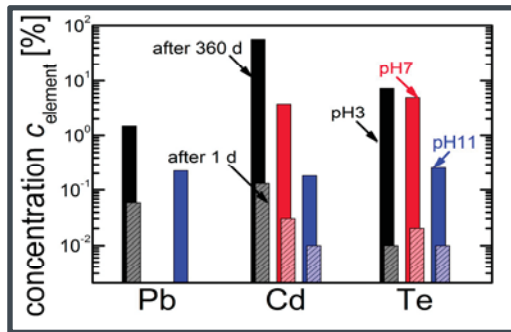
Nevertheless, it is not clear if these short leaching times allow meaningful predictions for the long term leaching behavior. Thus, our leaching experiments have lasted over 360 days without applying accelerating agitation to simulate more representative field conditions.

Our recently published study applied long term leaching on photovoltaic module pieces of 5 x 5 cm<sup>2</sup> size [1]. The pieces are cut out from modules of the four major commercial photovoltaic technologies: crystalline (c-Si) and amorphous silicon (a-Si), cadmium telluride (CdTe) as well as from copper indium gallium diselenide (CIGS). To simulate different environmental conditions, leaching occurs at room temperature in three different water based solutions with pH 3, 7 and 11. No agitation is performed. After 360 days, about 1.5% of lead (Pb) from crystalline silicon module pieces and almost 60% of cadmium (Cd) from cadmium telluride module pieces are leached out in acidic solutions. The leaching heavily depends on the pH, as well as the redox potential of the aqueous solutions, and, it increases with time.

Figure 1 shows a substantial difference between short and

long term leaching. Under all conditions, acid rain (pH3), groundwater (pH7) and alkaline landfilling (pH11), the amounts of eluted toxic elements as Pb, Cd and tellurium (Te) out of PV module pieces are much higher after one year than after one day. In neutral solutions, the long term results show an increase of nearly two orders of magnitude and for alkaline conditions an increase of more than one order of magnitude is found. For Cd and Te under acid rain conditions, the difference between short and long term is almost three orders of magnitude. For the leaching of Pb out of c-Si module pieces under acid rain conditions, an increase of more than 2000% is obtained.

**Figure 1:** Amount of eluted toxic elements as Pb, released from c-Si module pieces, and Cd and Te out of CdTe module pieces after  $t = 1$  day (hatched bars) and after  $t = 360$  days (solid bars) in solutions with pH3, pH7 and pH11.



Consequently, if the leaching amounts of the toxic substances Pb, Cd and Te from PV modules are low at the first day of leaching or lower than the regulatory limits according to standard tests, it is not likely that these values stay constant with ongoing leaching. Our study clearly proves that it is important to consider the long term behavior of leaching and the possibility that, after a certain time, 100% of the toxic material is leached out. To prevent environmental pollution due to a release of toxic heavy metals by dumping or landfilling broken PV modules, strict recycling policies and regulations are needed worldwide. Alternatively, toxic materials in PV modules simply could be omitted.

**Reference:**

[1] J. Nover, R. Zapf-Gottwick, C. Feifel, M. Koch, J.W. Metzger, and J.H. Werner, submitted to: Jpn. J. Appl. Phys. (2016)

## Laser Doping Approaches Auger Limit

Morris Dahlinger

In collaboration with: Kai Carstens

Laser doping of silicon is often linked to the formation of crystal defects or to the incorporation of impurities. These recombination centers could limit the performance of silicon microelectronic devices or the efficiency of solar cells. We show that there are no such recombination centers present in our laser doped silicon.

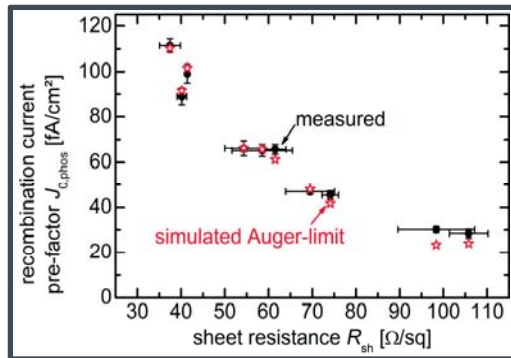
The *ipv* developed a laser doping process using phosphorus in a furnace grown phosphorus silicate glass (PSG) as dopant source. With this process, we reach the so called Auger-recombination limit in the doped regions. Symmetrically laser doped silicon samples are processed in a way that includes all relevant steps which we use for our laser processed back contact solar cells with efficiencies  $\eta = 23.24\%$  [1]. The recipe during the PSG growth and the pulse energy density during laser doping adjust the sheet resistance  $R_{sh}$  of the phosphorus doping. Both sample surfaces are passivated by hydrogenated amorphous silicon a-Si:H [2]. The recombination parameter  $J_{0,phos}$  of the laser doped samples is then extracted from photo conductance measurements. Electrochemical capacitance/voltage measurements determine the doping profiles of the same samples. The simulation tool PC1Dmod6.2 utilizes these doping profiles to simulate the recombination in the doped areas. The surface and the doped volume are assumed to be free of any Shockley Read Hall recombination (SRH), no defects are present. Since silicon is a semiconductor with indirect band gap, the radiative recombination is much less pronounced than the Auger-recombination, in particular for highly doped silicon. Therefore, this situation is called the Auger-limit.

Figure 1 shows the measured and simulated recombination current pre-factor  $J_{0,phos}$ . A reduced sheet resistance results

from higher doping concentration, thus higher charge carrier density, and consequently increased Auger-recombination and increased  $J_{0,phos}$ .

The simulated Auger-limit is in excellent agreement with the measured  $J_{0,phos}$ . Thus, there are no laser induced recombination centers detectable [3]. The presence of defects would result in a higher measured  $J_{0,phos}$  than the simulated Auger-limit. Furthermore, the experiment proves that a-Si:H excellently passivates the silicon surfaces.

**Figure 1:** Measured and simulated  $J_{0,phos}$  of laser doped silicon. The measured  $J_{0,phos}$  agrees excellently with the simulated Auger-Limit, thus no laser induced recombination is present.



The simulation of highly doped silicon like in our case depends on the accuracy of the available physical models, which are continuously refined. In highly doped silicon, some effects have to be accounted for, such as the band gap narrowing. The presented experiment not only shows that there are no laser induced defects, it also enables to test some of the widely spread models and reveals that the most common one does not accurately represent the physical reality. Therefore, our contribution helps to further increase the reliability of the simulation of highly doped silicon.

**References:**

[1] M. Dahlinger, and K. Carstens, E. Hoffmann, R. Zapf-Gottwick, and J.H. Werner, Prog. Photovolt: Res. Appl. **25**, 192-200 (2016).  
 [2] K. Carstens, and M. Dahlinger, J. Appl. Phys. **119**, 185303 (2016).  
 [3] M. Dahlinger, and K. Carstens, J. Appl. Phys. **120**, 155701 (2016).

## Between Infection and Rejection – Point-of-Care Testing of Immunosuppressants

Marcel Berner

In collaboration with: Sergej Vollmer, Markus Schubert

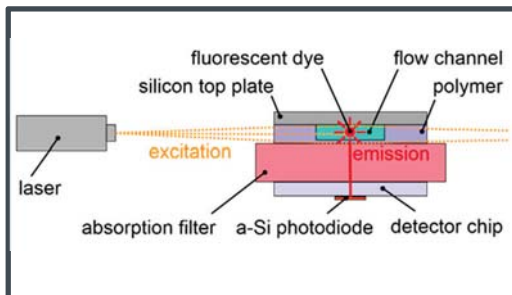
Rejection of transplanted organs is a severe health hazard for transplanted patients that is reduced by immunosuppressants. At the same time, however, those drugs enhance the risk of infections. Rapid changes of immunosuppressant levels in the patients' blood must be recognized for timely adjustment of dosing. Clinical routine as of today relies on one to few measurements of drug concentrations per day. Point-of-Care Testing with the new NANODEM (NANOphotonic DEvice for Multiple therapeutic drug monitoring) device enables quasi-continuous recording of critical drug concentrations every 20 minutes by blood sampling with a microdialysis catheter [1]. Our contribution to the European project NANODEM tailored and greatly improved the optoelectronic detection of fluorescent markers that label the immunosuppressants to be traced.

Key features of the optoelectronic fluorescence detection system include amorphous silicon (a-Si) based thin film photo-diodes for ultimate sensitivity [2], optimally integrated with low-noise electronic readout and side illumination of the microfluidic channels that carry the fluorescent labelled immunosuppressants in the free fraction of the patients' blood from microdialysis. A critical limitation of the sensitivity of NANODEM immunosuppressant monitoring arises from parasitic stray light at the excitation wavelength, originating from the monitored blood sample itself, the microfluidic channel, imperfections of the optical setup, and from magnetic nano-particles that enhance the fluorescence of analytes by applying sophisticated bioassay protocols.

Figure 1 depicts the optical setup for fluorescence detection from the volume of a microfluidic flow channel that is used

for homogeneous bioassays in the NANODEM project. In addition to photodiode manufacturing, *ipv* contributes the optical design of the side excitation, overall noise reduction and stray light rejection. Moreover, a very simple method for forming microfluidic channels from laser cut double-adhesive tape was developed with our project partners at the University of Tübingen.

**Figure 1:** Optical setup for fluorescence detection with laser excitation from the side of the channel. The absorption filter blocks remaining stray light from entering the a-Si photodiode at the bottom.



Since the analyte concentration and fluorescence signals are extremely low in this application, we measure a maximum photocurrent density  $J_{\text{photo}} = 10 \text{ nA cm}^{-2}$  in the a-Si photodiodes due to fluorescence from the flow channel. Dark current density of  $11 \times 3.3 \text{ mm}^2$  sized a-Si detectors is as low as  $J_{\text{d}} = 100 \text{ fA cm}^{-2}$ , close to the thermal background limit. Taking into account the available sampling time of  $t_s = 100 \text{ s}$ , an overall assessment of the limit of detection of the final NANODEM Analyser reveals a minimum detectable fluorescence intensity  $I_{\text{min}} = 4.5 \text{ pW cm}^{-2}$  with a dynamic range of 78 dB. Thereby, a minimum concentration of 26 nmol/L of our reference dye DY-636 can be traced in pure water by this direct optical test format.

First clinical tests of the NANODEM Point-of-Care Testing system will start in Munich in early 2017, after successful approval by the ethics committee in December 2016.

### References:

- [1] <http://nanodem.ifac.cnr.it/index.php/project-overview>
- [2] M. Berner, R. Rothmund, S. Vollmer, M. Schubert, U. Hilbig, and G. Gauglitz, *phys. stat. sol. A*, 1862-6319 (2016), DOI: 10.1002/pssa.201532953.

# Electrical Contact Resistance of Clamped Battery Cells

Christoph Bolsinger

In collaboration with: Matthias Zorn, and Kai Peter Birke

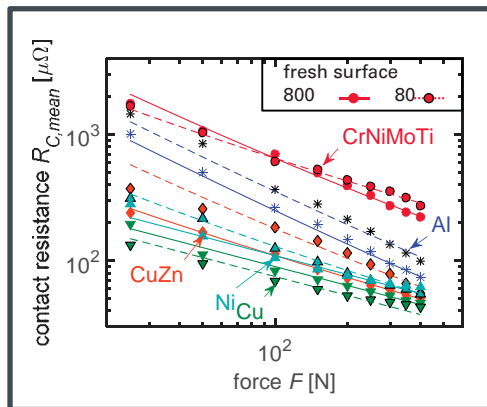
The electrical contact resistance (ECR), which occurs at the contact interface, is one of the crucial criteria to design a battery cell joint. A poor connection with an increased contact resistance leads to a significant heat generation and subsequently causes a heat transfer into the battery cell. Currently, welding processes such as resistance spot, ultrasonic or laser beam welding are commonly used to interconnect battery cells [1]. Besides the heat input during the welding process a huge drawback of welded battery cell connections is the complex disassembling process. An easy way to assemble and disassemble battery cells without damaging is the use of clamped cell connectors.

The present study investigates the ECR of clamped cell connectors for 18650 battery cells. A positive terminal of a Panasonic NCR18650B Li-Ion cell is used for ECR measurements and for an investigation of the mechanical properties. A load test indicates that the positive terminal undergoes an elastic deformation up to a force of about 400 N and can therefore be used for clamped joints without any damage. To investigate the dependencies of ECR, the applied force on the joint is varied from 25 to 400 N. Five different materials with three different surface roughnesses are used as cell connectors. Furthermore, the influence of aged surfaces are investigated. The obtained data show, that the ECR of clamped cell connectors is reduced to about 50  $\mu\Omega$ . Thus, the ECR is in the range or even lower than for welded contacts [2].

Figure 1 shows the mean values of the measured electrical contact resistances  $R_{c,mean}$  in dependence of the applied force  $F$  and the surface treatments with different grit size of the abrasive paper.

The specific lines describe the ECR as a function of the resistivity, hardness and surface roughness of the material as well as the contact area and the applied force. For all grit sizes, CrNiMoTi shows the highest resistance compared to the remaining materials. The contact elements made of copper show for all grit sizes the lowest ECR. The ECR slightly varies with the roughness of the surface. For all materials except copper, the ECR increases with increasing roughness  $R_a$  in range of  $F > 100$  N. The lowest ECR is obtained by an applied force of  $F = 400$  N.

**Figure 1:** Electrical contact resistances  $R_{c,mean}$  for different contact materials. The surface treatment is done with an abrasive paper with a grit size of 80 and 800. For all contact materials (except Cu) the resistances slightly increase with increasing surface roughness  $R_a$ . At a force of 400 N the ECR of all contact materials is in the range or even lower than for welded contacts.



Furthermore, the influence of the contact area and the film resistance due to oxidation on the ECR are investigated. The contaminant films strongly increase the ECR for low contact forces. The measurement results show that the selection of the contact material (low resistivity and low hardness) is crucial to achieve low ECR. Surface roughness as well as the clamping area have less influence.

### References:

- [1] S.S. Lee, T.H. Kim, and S.J. Hu, ASME 2010 Int. Manuf. Sci. Eng. Conf. Proc. **1**, 541–549 (2010).
- [2] M.J. Brand, P.A. Schmidt, and M.F. Zaeh, J. Energy Storage **1**, 7–14 (2015).

## 23.3% Back Contact Solar Cells with Amorphous Silicon Passivation

Kai Carstens

In collaboration with: Morris Dahlinger, Erik Hoffmann, Renate Zapf-Gottwick, and Jürgen Werner

High efficiency solar cells like interdigitated back contact (IBC) solar cells feature both doping types on the rear side of the cell: the phosphorus doped back surface field (BSF) as well as the boron doped emitter. High quality passivation of heavily boron doped p-type crystalline silicon (c-Si) is usually achieved with aluminum oxide, via low interface state density and a high amount of negative fixed charges [1]. For heavily phosphorus doped n-type surfaces silicon nitride, with positive fixed charges, is used [2]. Applying e.g. only aluminum oxide to both doping types, will result in a detrimental passivation of the phosphorus doped back surface field; therefore the phosphorus doped area needs to be reduced [3]. In any case, the passivation of heavily p-type and n-type doped surfaces is a challenge on the way to achieve high efficiencies. One possibility is to use two different passivation layers and structure them according to the surface doping. However, the ultimate solution lies in using a universal passivation layer for both doping types.

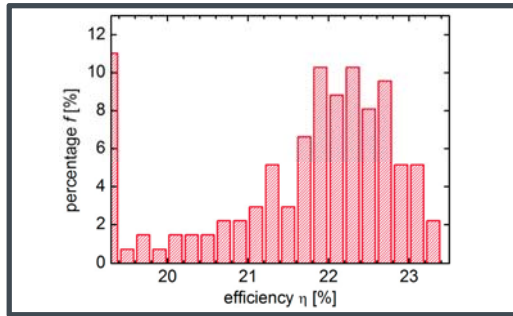
We use amorphous silicon (a-Si:H) as passivation layer for both, heavily phosphorus, and boron doped surfaces. a-Si:H applied to our IBC solar cells, yields an efficiency  $\eta = 23.3\%$ .

Excellent passivation of boron and phosphorus doped surfaces is achieved by optimization of the deposition conditions [4]. The recombination parameter  $J_{0,Em} = 29 \text{ fA/cm}^2$  is typical for a boron doped emitter with sheet resistance  $R_{sh,Em} = 82 \text{ } \Omega/\text{sq}$ . The phosphorus back surface field with sheet resistance  $R_{sh,BSF} = 54 \text{ } \Omega/\text{sq}$  yields a recombination parameter  $J_{0,BSF} = 44 \text{ fA/cm}^2$ . Both values are close to the Auger-limit.

We integrate the a-Si:H passivation into our laser processed IBC solar cells. Both doping types are prepared using laser doping [5]. For the passivation we remove the silicon oxide

(which is usually used as rear side passivation) in hydrofluoric acid. Then, we deposit 30 nm a-Si:H at optimized deposition conditions. Laser ablation locally removes the passivation layer for contact formation. Finally, structuring of the aluminium metallization is also done with a laser process. Figure 1 shows the distribution of the efficiency  $\eta$  of 136 laser processed solar cells with an area  $A = 4 \text{ cm}^2$ . The best solar cell has an efficiency  $\eta = 23.3\%$  with open circuit voltage  $V_{oc} = 684 \text{ mV}$ , short circuit current density  $J_{sc} = 41.5 \text{ mA/cm}^2$  and fill factor  $FF = 81.9\%$ .

**Figure 1:** Efficiency histogram for 136 laser processed IBC solar cells. Maximum efficiency  $\eta = 23.3\%$ , median efficiency  $\eta = 22.1\%$



The excellent passivation of heavily doped boron emitter and phosphorous back surface field with undoped amorphous silicon helps to increase the solar cell area. Additionally to the small area cells, we also manufactured a large solar cell with  $\eta = 22.6\%$  on an area  $A = 156 \text{ cm}^2$ . Next, we will scale up the cell size further to  $A = 239 \text{ cm}^2$ , continuing to fabricate modules made of these cells.

### References:

- [1] B. Hoex, J. Schmidt, R. Bock, P.P. Altermatt, M.C.M. van de Sanden, and W.M.M. Kessels, *Appl. Phys. Lett.* **91**,112107 (2007).
- [2] M.J. Kerr, J. Schmidt, A. Cuevas, and J.H. Bultman, *J. Appl. Phys.* **89**, 3821 (2001).
- [3] R. Müller, C. Reichel, J. Schrof, M. Padilla, M. Selinger, I. Geisemeyer, J. Benick, and M. Hermle, *Sol. Energ. Mat. Sol. Cells.* **142**, 54 (2015).
- [4] K. Carstens, and M. Dahlinger, *J. Appl. Phys.* **119**, 185303-1 (2016).
- [5] M. Dahlinger, K. Carstens, E. Hoffmann, R. Zapf-Gottwick, and J. H. Werner, *Prog. Photovolt: Res. Appl.* **25**, 192 (2016).

# Laser Processed Refraction Gratings for Improved Light Trapping in Solar Cells

Mohamed Hassan

In collaboration with: Morris Dahlinger,  
and Jürgen Köhler

Refraction gratings on the rear side of solar cells improve the light trapping properties of solar cells. The longer the wavelength of radiation becomes, the more the diffraction angle increases. Therefore, photons with energy near the band gap of a semiconducting material have the longest optical path length. Different one- [1] and two-dimensional [2] diffractive grating structures were already studied. The disadvantage of those structures is the costly and time consuming manufacturing process using photo-lithography. This work presents a new, cost-efficient method for the generation of a periodic back surface texture on the rear side of crystalline silicon solar cells.

Figure 1 shows a laser microscope picture of a periodic back surface texture using a nanosecond-pulsed laser of wavelength  $\lambda = 532$  nm. Here, a purpose designed focusing optics transforms the laser beam to a top-hat line focus of size  $10 \mu\text{m} \times 800 \mu\text{m}$ . The absorption of the laser radiation leads to rapid heating and subsequent melting of the silicon surface. The line focus melts an about  $7 \mu\text{m}$  wide and  $500$  nm deep stripe of silicon. Liquid silicon has a significantly larger density than solid silicon. This density anomaly leads to a strongly curved surface of the liquefied silicon stripe. The strong curvature of the liquid surface, together with the surface tension, leads to the formation of a so-called capillary surface wave, travelling through the liquid until it freezes when re-solidifying. The result is a periodically textured surface on a laser processed silicon wafer. The "wavelength" of the periodic structure is easily adjusted by varying the pulse repetition frequency and/or the scanning speed of the laser beam focus.

As shown in figure 1, the period of the resulting gratings is in the order of micrometers with an amplitude of up to 300 nm.

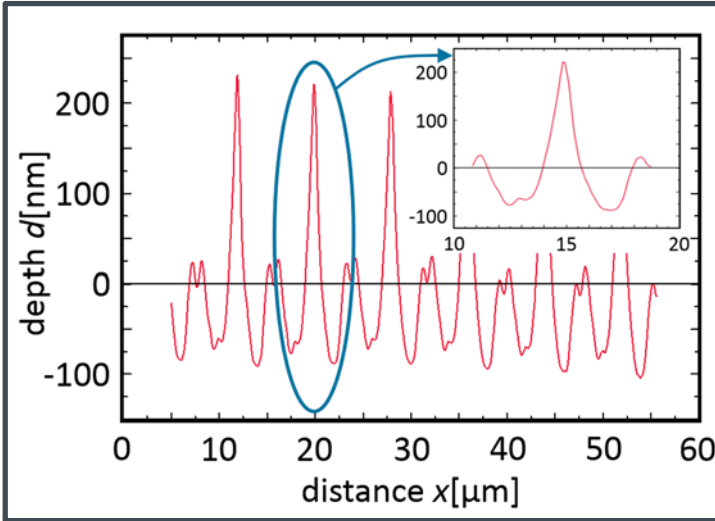


**Figure 1:** Laser microscope picture of the periodic structure on a silicon wafer processed with a line-focused pulsed laser beam of wavelength  $\lambda = 532$  nm.

Future work will investigate the ability of these structure to improve solar cells light trapping for near bandgap radiation.

### References:

- [1] A. Mellor, H. Hauser, C. Wellens, J. Benick, J. Eisenlohr, M. Peters, A. Guttowski, I. Tobías, A. Martí, A. Luque, and B. Bläsi, *Optics Express* **21**, A295 (2013).
- [2] M. Peters, M. Rüdiger, H. Hauser, M. Hermle, and B. Bläsi, *Prog. Photovolt: Res. Appl.* **20**, 862 (2012).

# High Resolution Carrier Lifetime Imaging

Timo Kropp

In collaboration with: Markus Schubert  
and Jürgen Werner

Over the last years, minority carrier lifetime imaging has become a standard tool for solar cell characterization [1,2]. High spatial resolution of such images and fast throughput are contradictory requirements for quality control in photovoltaic production. To solve this conflict, we present a novel technique for high resolution mapping for the effective minority carrier lifetime  $\tau_{\text{eff}}$  of solar cells.

The technique relies on using electroluminescence (EL) measurements with two different modulations. The intensity difference  $\Delta r$  between two differently modulated EL images depends on the minority carrier lifetime. A Si CCD (charge coupled device) camera takes one image during a pulsed current modulation a) with a step-function change from forward- to reverse-bias conditions. A second image is taken during the modulation with a step-function change from b) forward-bias to open-circuit. By calculating the intensity difference  $\Delta r$  between these two images, we find a solution for the effective minority carrier lifetime

$$\tau_{\text{eff}} = \frac{\Delta r t_p}{M \ln(1 + M^{-1})} \quad (1)$$

with the intensity difference  $\Delta r$ , the period length  $t_p$  of the current modulations and the modulation  $M = I_r/I_f$  given by the ratio of the forward-bias current  $I_f$  and the reverse-bias current  $I_r$ .

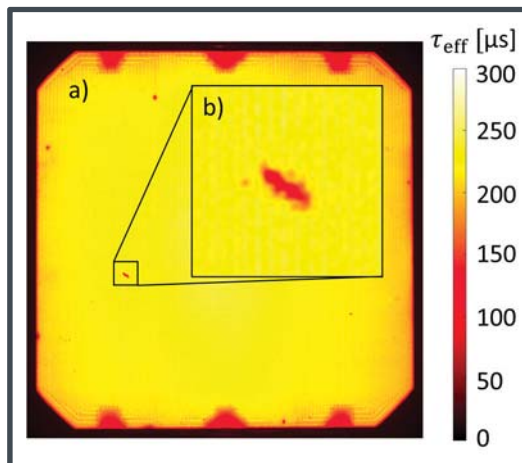
The luminescence intensity in the image, while modulating the current injecting under forward-bias, is based on free carrier recombination. In contrast, images taken while actively extracting excess charge carriers in reverse-bias show reduced intensity due to the increased fall time of the signal. This mode of operation leads to asymmetric luminescence

rise and decay times, which allows to determine the carrier lifetime from EL images acquired over several modulation periods.

Instead of averaging multiple high speed images, taken from one modulation period within microseconds, single images with long exposure times up to minutes prove to be useful for lifetime mapping. Therefore, low-cost and “slow” Si CCD cameras can be used for imaging and deducing the minority carrier lifetime map.

Figures 1a,b show first results of the novel lifetime mapping technique calculated by eq. (1). The enhanced view in Fig. 1b) is cropped from the original image in Fig. 1a). Usually, this sort of detailed analysis is only possible by changing the optics of a measurement setup.

**Figure 1:** High resolution effective carrier lifetime image (a) of a Sunpower IBC (interdigitated back contact) solar cell, and (b) enhanced view of a damaged area. The high resolution of (a) allows to characterize defects over the total cell area in only one image without taking multiple high speed images.



However, in our case, the high resolution of Fig. 1a) allows to identify defects over the total cell area in only one image without changing the optics.

### References:

- [1] S. Herlufsen, K. Bothe, J. Schmidt, R. Brendel, and S. Siegmund, *Sol. En. Mat. Sol. Cells* **106**, 42 (2012)
- [2] K. Ramspeck, K. Bothe, J. Schmidt, and R. Brendel, *J. Appl. Phys.* **106**, 114506 (2009)

## Low Pressure Glow-Discharge Methanation

Friedrich-Wilhelm Speckmann

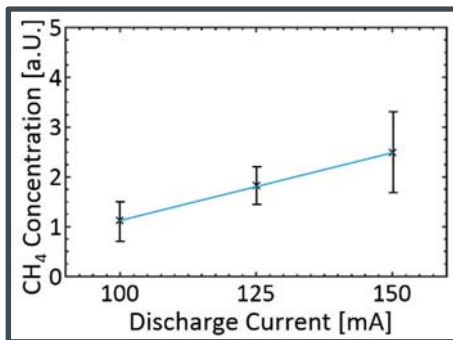
In collaboration with: Jürgen Köhler,  
Daniel Müller and Kai Peter Birke

Plasma technology is gaining increasing interest for the reduction of carbon dioxide ( $\text{CO}_2$ ) to carbon monoxide ( $\text{CO}$ ) and oxygen ( $\text{O}_2$ ) [1]. The  $\text{CO}$  gas and hydrogen ( $\text{H}_2$ ) are ideal reaction partners to produce hydrocarbons, like gas and fuel. The aim of our research is to investigate a new method to produce methane ( $\text{CH}_4$ ) by plasma induced dissociation of  $\text{CO}_2$  and  $\text{H}_2$  in a single setup. A low pressure glow discharge plasma dissociates  $\text{CO}_2$  into  $\text{CO}$  and  $\text{O}_2$  and a cathode-integrated zirconia based ion conductor transports oxygen ions ( $\text{O}^{2-}$ ) in or out of the reaction chamber, depending on the direction of the applied "transport voltage". The bi-directional transport properties of zirconia enables two unique features: i) transporting oxygen ions into the reaction chamber enables to control the partial pressure of water vapor in the reaction chamber, ii) a transport of oxygen atoms in the opposite direction reduces the amount of oxygen molecules and, consequently decreases the recombination of  $\text{CO}$  and  $\text{O}_2$ , resulting in an improved  $\text{CO}_2$  conversion rate. The operating temperature of the ion-conducting zirconia can be varied using an electric heater. We observe a strong influence of operating temperature on the conversion rates of  $\text{CH}_4$  and  $\text{CO}$ . Increasing the zirconia temperature results in lower  $\text{CO}$  but higher  $\text{CH}_4$  conversion rates [2].

The applied voltage  $V_{\text{Pr}}$  to our zirconia ion conductor,  $-7.5 \text{ V} < V_{\text{Pr}} < 7.5 \text{ V}$ , and the magnitude of the discharge current have a major impact on the amount of  $\text{O}^{2-}$  ions flowing into or out of the reaction chamber. Increasing the discharge current  $I_{\text{PL}}$  leads to more extracted  $\text{O}^{2-}$  ions and, at the same time, to increased  $\text{CO}$  production.

The correlation between  $I_{pL}$  and amount of gas can also be observed for the  $\text{CH}_4$ . We analyze the composition of the gas in our reaction chamber using a gas-phase chromatograph. Figure 1 shows a linear dependency of the  $\text{CH}_4$  peak area on the discharge current  $I_{pL}$ . The amount of synthesized methane increases by a factor of two between  $100 \text{ mA} < I_{pL} < 150 \text{ mA}$ . The higher yield of methane is caused by the bigger discharge plasma volume leading to more ionized  $\text{CO}_2$  and  $\text{H}_2$  gas.

**Figure 1:** Methane concentration in the reaction chamber with discharge currents  $I_{pL} = 100 \text{ mA}$ ,  $125 \text{ mA}$  and  $150 \text{ mA}$ , measured using a gas-phase chromatograph.



Especially, the combination between the optimal zirconia temperature needed for the methanation and the simultaneous water electrolysis by an oxygen ion conductor are of future interest and can further boost the amount of synthesized methane from hydrogen.

Future research will also focus on the pre-required hydrogen generation. Experiments with a newly designed, transistor-based power source aim to increase the performance of an alkaline electrolyzer. Improved performance is expected with respect to maximum throughput and partial load operation, using modified current profiles.

#### References:

- [1] R. Aerts, W. Somers, and A. Bogaerts, *ChemSusChem* **8**, 702-716 (2015).
- [2] F. Speckmann, D. Müller, J.R. Köhler, and K.P. Birke submitted to: *J. CO<sub>2</sub> Util.* (2016).

# Series Resistance Mapping of Back Contact Solar Cells

Osama Tobail

In collaboration with: Erik Hoffmann,  
Renate Zapf-Gottwick, and Jürgen Werner

We determine the spatial distribution of the series resistance  $R_s(x, y)$  of interdigitated back contact (IBC) solar cells as a function of the  $x$  and  $y$  coordinates by means of luminescence imaging  $\phi(x, y)$ . A cooled silicon CCD camera captures the electroluminescence (EL) images of the solar cell in the dark at variable terminal voltages  $0.55 \text{ V} > V > 0.7 \text{ V}$  in steps  $\Delta V = 10 \text{ mV}$ . In addition, we use a high pass filter ( $\lambda_c = 815 \text{ nm}$ ) to suppress any stray light. Before we calculate the series resistance from the EL images, we subtract a background image. The camera has a  $1024 \times 1040$  pixel array used to image a solar cell with an area of  $12.5 \times 12.5 \text{ cm}^2$ , which results in an area  $a = 120 \times 122 \text{ }\mu\text{m}^2$  of the cell imaged by each pixel. The exposure time of the camera in this experiment equals  $2.5 \text{ s}$  for each EL-Image, while four Peltier elements and a Peltron™ controller keeps the cell temperature  $T_{\text{cell}} = 25 \text{ }^\circ\text{C}$  constant during the whole experiment. Each measurement is repeated four times and averaged to minimize errors.

We use the analysis developed by Hinken *et al.* [1] and inspired by the Werner plot [2]. The advantage of this method is that it is based on the linear fit of the equation

$$\frac{V_t}{\phi(x, y)} \frac{d\phi(x, y)}{dV} = b(x, y) \left[ 1 - \frac{R_s(x, y)}{CJ} \phi(x, y) \right] \quad (1)$$

with  $V_t = 26 \text{ mV}$ , the thermal voltage at room temperature, and the fit-parameters  $b(x, y)$  and  $CJ$ . We determine for each pixel  $R_s(x, y)$ ,  $b(x, y)$  and  $CJ$  as in Ref [1].

This method is applied for the first time for IBC cells, therefore, we validated it on the three dimensional Quokka [3] simulation of our IBC cells.

Figure 1a shows the EL-image at  $V = 0.7 \text{ V}$  as an example. Regions with high EL intensity indicate that the local voltage

is high due to the exponential voltage dependence of EL intensity [1]. Low intensities and hence low local voltages result from either an elevated series resistance or local high recombination. Equation (1) separates the series resistance effect from the recombination effects. If the low intensity is originating from local high recombination or parallel resistance, this will influence the parameters  $CJ$  or  $b(x, y)$ , while, if the series resistance is responsible, the decreased intensity,  $R_s(x, y)$  will be determined [1].

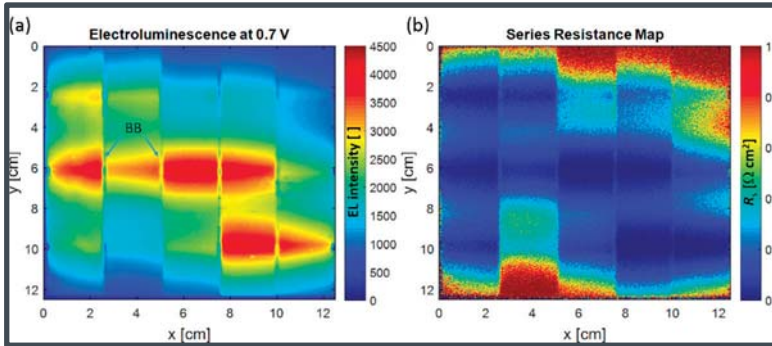


**Figure 1:** a) Electroluminescence image at  $V = 0.7 \text{ V}$  for an IBC solar cell. The cell has six bus-bars on back side. b) Resulting  $R_s$  map with a global resistance of  $0.1 \Omega \text{ cm}^2$ .

Figure 1b illustrates the local series resistance  $R_s$ . The resulting map shows an elevated series resistance  $R_s$  on the cell edges, especially the upper right corner. The EL-image in figure 1a at its own cannot give this information. In figure 1a, both of edges of the cell and the back side bus-bars (BB) show low EL signal, while only the edges show elevated  $R_s$ . We determine the global series resistance  $R_{s,\text{global}} = 0.1 \Omega \text{ cm}^2$  from the map as the parallel equivalent of all local resistances. The  $R_{s,\text{global}}$  agrees well with the series resistance  $R_{s,J/V} = 0.12 \Omega \text{ cm}^2$  determined from current/voltage-curve according to the Werner method [2].

### References:

- [1] D. Hinken, K. Ramspeck, K. Bothe, B. Fischer, and R. Brendel, *Appl. Phys. Lett.* **91**, 182104 (2007).
- [2] J. H. Werner, *Appl. Phys. A* **47**, 291 (1988).
- [3] A. Fell, K. C. Fong, K. R. McIntosh, E. Franklin, and A. W. Blakers, *IEEE J. Photovolt.* **4**, 1040 (2014).

# Anomalous Boron Segregation in Liquid Silicon

Patrick Lill

In collaboration with: Morris Dahlinger,  
and Jürgen Köhler

Pulsed laser melting, which is the key feature of the patented *ipv* laser doping process, is also valuable for fundamental research on rapid solidification of silicon (Si) with dopant incorporation. Laser doping bases on the diffusion of dopant atoms in locally laser-melted Si, which form doped regions via epitaxial re-crystallization after the laser irradiation.

Due to the localized heat input during laser doping, large temperature gradients between the Si melt and the surrounding solid develop, which lead to high solidification velocities. The rapid solidification leads to non-equilibrium crystallization at the advancing liquid/solid phase interface, causing dopant concentrations in the just formed Si solid which do not match their equilibrium values. The ratio of dopant concentrations directly at the liquid/solid interface defines the partitioning (or segregation) coefficient  $k_p = C_s/C_l$ , with the concentrations in the Si crystal  $C_s$  and melt  $C_l$ .

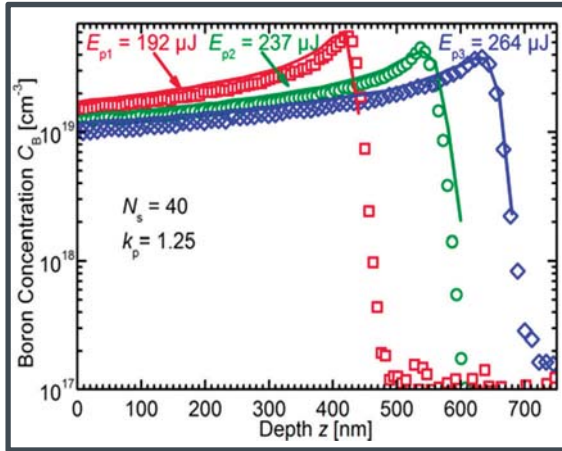
We investigate the boron (B) incorporation and redistribution during repeated laser melting and observe a distinct B pile-up around the maximum melt depth for repeated laser melting cycles. The equilibrium values of the partitioning coefficient for B in Si is  $k_{eq} = 0.8$ , which means that B atoms segregate into the melt at the advancing liquid/solid interface.

In contrast, we determine a partitioning coefficient value  $k_p = 1.25$  by means of a numerical model which reproduces the experimental boron profiles remarkably well. For high solidification (interface) velocities, the segregation/partitioning of dopants into the melt can be suppressed, this phenomenon is denoted solute trapping with  $k_p$  approaching unity ( $k_p = 1$  for complete solute trapping). In the classical solute trapping models, a partitioning/segregation coefficient

above unity is not possible, thus we term this behavior anomalous segregation.

Figure 1 shows the B concentration profiles measured with secondary ion mass spectroscopy (SIMS) for three pulse energies  $E_{p1} = 192 \mu\text{J}$ ,  $E_{p2} = 237 \mu\text{J}$ ,  $E_{p3} = 264 \mu\text{J}$  and constant number of laser scans  $N_s = 40$ , together with the respected simulated profiles.

**Figure 1:** Measured (open symbols) and simulated (lines) boron concentration profiles for three laser pulse energies  $E_{p1} = 192 \mu\text{J}$ ,  $E_{p2} = 237 \mu\text{J}$ ,  $E_{p3} = 264 \mu\text{J}$  and constant number of laser scans  $N_s = 40$ . The simulation fits the data remarkably well for a partitioning coefficient  $k_p$  above unity with  $k_p = 1.25$ .



Our approach offers a simple and straightforward procedure to determine the partitioning coefficient from experimental results. A partitioning coefficient above unity is consistent with the assumption of an adsorptive liquid/solid interface which attracts B atoms and, in conjunction with a high solidification velocity leads to an increased B concentration in the just formed Si right behind the interface. Repeated re-crystallization cycles enhance this effect and cause the reported pile-up near the maximum melt depth.

These results [1] indicate the requirement for an extended model to describe the boron pile-up within the solute trapping framework.

**Reference:**

[1] P.C. Lill, M. Dahlinger, and J.R. Köhler, submitted to: mmpi Materials (2016).

# STROMBANK: Innovation for Local Energy Storage

Timo Kropp

In collaboration with: Markus Schubert,  
Thomas Wurster, Jürgen Werner,  
and Thomas Speidel (ads-tec)

The economic model of a bank that manages financial transactions in money accounts is well-known. This banking approach serves as a model for the "Electricity Bank" (STROMBANK) research project [1]. The STROMBANK manages the increasing amount of renewable and decentralized electricity generation in the low-voltage grid by customers, who are consumers as well as producers at the same time, so-called prosumers. At best, renewable electricity is consumed or temporarily stored in the vicinity of its generation site. As a consequence, load and losses of electricity distribution grids go down, since the amount of energy transformed and transmitted is lowering.

The innovative STROMBANK approach enables time-shifting and temporal matching of each prosumer's own production and consumption. All account holders are able to share and trade their banked electricity among each other, with neighbors, or even to the electricity stock exchange.

The main incentives for sharing a neighborhood battery storage are economic benefits for the prosumers as well as the operators of such battery containers. Consequently, they gain the ability of providing grid services like balancing reserve.

Figure 1 outlines the system layout of the STROMBANK test installation. The STROMBANK is a 100 kWh Li-ion battery storage [2] connected to the local low-voltage grid. Generation and consumption meters record the data of thirteen photovoltaic (PV) and three combined heat and power (CHP) systems, all with nominal output powers around 5 kW. The 100 kWh Li-ion battery storage is connected to the local grid, being charged and discharged with the residual energy flow of all STROMBANK prosumers. We evaluate the individual electricity consumption and production data, plus the overall STROMBANK traffic, and model the complete system.

Thereby we calculate and optimize the energy balance of the STROMBANK, without the need of direct physical wire connections during this evaluation phase.

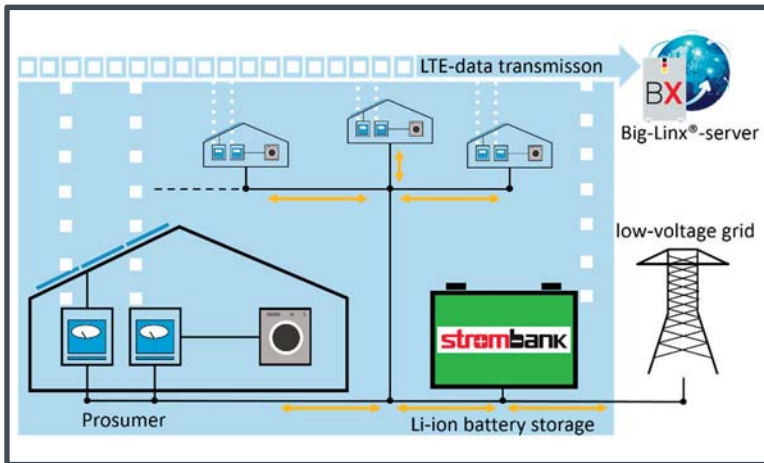


**Figure 1:** The STROMBANK prosumers share the total capacity of the Li-ion battery container, each with his individual energy (bank) account.

Evaluating all energy flows on a 5-seconds time base, proves an approximate doubling of the self-consumption rate of the PV prosumers to an average 61% when using their STROMBANK electricity storage account. Seasonal allocation of storage capacity, i.e. STROMBANK account size, makes best use of the PV and CHP power generation, which is nicely complementary during the course of a year. Even higher self-consumption rates > 95% are possible in the very same scenario by dynamic account size allocation that is optimized for maximum energy throughput, i. e. for most economic usage of the total storage capacity [3].

### References:

- [1] Final report: <<http://www.fachdokumente.lubw.baden-wuerttemberg.de/servlet/is/120150/?COMMAND=DisplayBericht&FIS=203&OBJECT=120150&MODE=METADATA>>
- [2] <http://www.ads-tec.de/en/energy-storage.html>
- [3] T. Kropp, J. Wang, M. Schubert, and J.H. Werner, in *Proc. of the 5th International Education Forum on Environment and Energy Science* (2016); DOI: 10.13140/RG.2.2.11150.36162

## Mechanical Stress in Lithium-Ion Batteries

Jan Patrick Singer

In collaboration with: Kai Peter Birke

Lithium-ion cells are state of the art technology for electrical energy storage in mobile as well as stationary battery systems. They offer high power and energy densities, low self-discharge rates, high efficiencies, low toxicities and high lifetimes. Considering the lifetime, not all ageing mechanisms are fully understood.

During the charging process of a lithium-ion cell, positive ionic charge carriers  $\text{Li}^+$  intercalate into the negative electrode (anode). The common anode material is graphite  $\text{C}_6$  showing a volume strain  $\Delta V/V_0 = 12.8\%$  during Li-insertion [1]. At the same time, the positive electrode (cathode) releases the  $\text{Li}^+$  ions under a negative volume strain  $\Delta V/V_0 = -6.6\%$  for lithium iron phosphate  $\text{LiFePO}_4$  [1]. The total volume strain is measured as a change of force which is applied externally on the cell. Ageing investigations show, that the cyclic lifetime of a pouch cell extends by applying an external force [2]. Additionally, measuring the cell's pressure can be used for State of Charge (SoC) prediction and State of Health (SoH) diagnostics. For both, SoC prediction and SoH diagnostics, pressure change processes and their variation over the lifetime of the cell need to be understood.

Figure 1 shows one charge and discharge cycle of a  $\text{LiFePO}_4/\text{C}_6$  cell. Since  $\text{LiFePO}_4$  follows a two-phase transition mechanism for lithiation, the voltage characteristic (blue line) shows a flat plateau over a wide range of SoC. The red line represents the charge, respectively discharge current. In charge direction, the force  $F$  in green follows the trend of voltage  $V$ . However, in discharge direction, a non-monotonic slope of  $F$  is noticeable.

During the discharge process, the  $\text{LiFePO}_4$  transforma-

tion follows the equation



When the concentration of transformed particles reaches a critical state with a concentration instability the chemical potential of Lithium  $\mu_{\text{Li}}$  drops [3]. The drop  $\mu_{\text{Li}}$  of results in a flat voltage plateau and a intermediate rise of the measured force  $F$ .

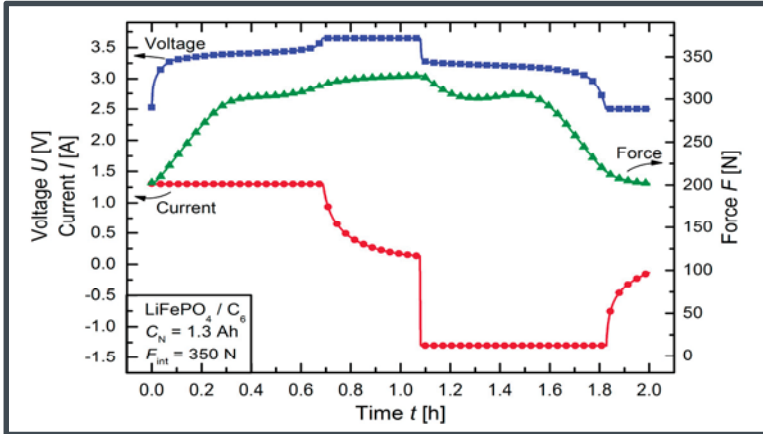


**Figure 1:** Voltage characteristic of  $\text{LiFePO}_4/\text{C}_6$  pouch cell measured during one charge and discharge cycle (blue line). The cell is charged respectively discharged with a constant current  $I_{\text{CC}} = 1\text{C}$  until the cut-off voltage is reached followed by constant voltage charging until the currents drops below  $I_{\text{CV}} < 1/100\text{C}$ . The red line shows the corresponding current  $I$  and the green line the measured Force  $F$  with an initial Force  $F_{\text{int}} = 350\text{N}$  at  $\text{SoC} = 100\%$ . The nominal capacity of the cell is  $C_N = 1.3\text{Ah}$ .

The phase transition, influencing the external force and thereby the aging process is still not completely explained by common theories and recently studied at the *ipv*. Based on particle models, we describe the trend of  $\mu_{\text{Li}}$  and predict the aging process of  $\text{LiFePO}_4/\text{C}_6$  cells as a function of force  $F$ .

### References:

- [1] W.H. Woodford, W.C. Carter, and Y.-M. Chiang, *Energy Environ. Sci.* **5**, 8014 (2012).
- [2] J. Cannarella, and C.B. Arnold, *J. Pow. Source* **245**, 745 (2014).
- [3] R. Malik, A. Abdellahi, and G. Ceder, *Electrochem. Soc.* **160**, A3179 (2013).

# Chemical Stability of Cadmium Telluride Powder

Renate Zapf-Gottwick

In collaboration with: Jessica Nover, Matthias Zorn, Caroline Feifel<sup>1</sup>, Michael Koch<sup>1</sup>, and Jürgen Werner

<sup>1</sup>Institute for Sanitary Engineering, Water Quality, and Solid Waste Management, University of Stuttgart, Germany

The crystalline compound cadmium telluride (CdTe) is known as a direct II-VI semiconductor and as material for solar cells and optical detectors. However, cadmium is highly toxic and forbidden in most products (still not in photovoltaics). Cadmium telluride usually is assumed to be chemically stable. Only strong acids should be able to decompose the bonding of CdTe. Our recently published study showed an elution of cadmium and tellurium out of CdTe photovoltaic module pieces not only in acidic solutions [1]. Here, we present elution experiments for different grain sizes of CdTe powder. The result is: the smaller the grain size, the higher the instability and the decomposition of CdTe. However, the thickness of the CdTe layer in modules is smaller and shows the highest elution out of milled CdTe modules [2].

Our experiments are carried out on commercially available CdTe powder. We use powder with different given maximum particle sizes (due to sieving) characterized by their diameter  $d$ : (i) CdTe<sub>250</sub> with  $d_{250} \leq 250 \mu\text{m}$ , (ii) CdTe<sub>840</sub> with  $d_{840} \leq 840 \mu\text{m}$ , and (iii) CdTe<sub>3000</sub> with  $d_{3000} \leq 3000 \mu\text{m}$ . We compare the results with leaching results of a former study on milled CdTe modules  $Cd_{3,m}$  with a thickness  $d_{CdTe,m} \approx 3 \mu\text{m}$ .

The leaching experiments are carried out at room temperature. To secure constant pH values, we utilize buffered solutions. We leach the different CdTe powder in three water based solutions with pH4, pH7, and pH10. Inductively coupled plasma mass spectroscopy analyzes the amount of dissolved substances but no precipitations. We carry out the experiments three times and show the results as mean values. The measurement uncertainty is around +/-10%.

Figures 1a and b show the time dependent elution of Cd and Te with respect to their total mass. The smaller the size of the used CdTe powder, the higher is the amount of eluted Cd in solutions with pH4, as illustrated in fig. 1a:  $Cd_{m,3} > Cd_{p,250} > Cd_{p,840} > Cd_{p,3000}$ . Figure 1b demonstrates the higher elution of Te, now in solutions with pH7, with smaller sizes of the powder:  $Te_{m,3} > Te_{p,250} > Te_{p,840} > Te_{p,3000}$ .

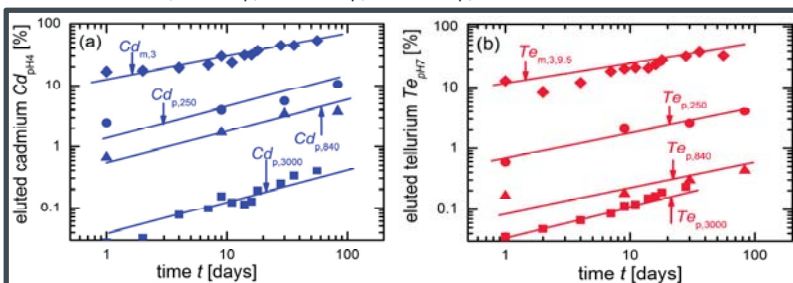


**Figure 1:** Stability of CdTe shown by a) elution of Cd out of CdTe powder in solutions with pH4:  $Cd_{m,3} > Cd_{p,250} > Cd_{p,840} > Cd_{p,3000}$  [1] and b) elution of Te out of CdTe powder in solutions with pH7:  $Te_{m,3} > Te_{p,250} > Te_{p,840} > Te_{p,3000}$ . Lines in the diagrams are guides for the eye.

The elution of Cd reduces by about one order of magnitude whenever the pH-value increases from 4 to 7 and further to 10. The elution of Te from  $Te_{m,3}$  is more or less independent from the pH-value while  $Te_{p,250}$ ,  $Te_{p,840}$ , and  $Te_{p,3000}$  out of powder becomes smaller with higher pH.

Our experiments prove the chemical instability of CdTe to depend on the size of the CdTe powder and the pH values of the aqueous solutions. In more acidic solutions, Cd and Te dissolve. In contrast, in solutions with higher pH, neutral or alkaline, the compound dissolves by the release of Te only, while the element Cd precipitates probably as cadmium hydroxide [2].

**References:**

[1] J. Nover, R. Zapf-Gottwick, C. Feifel, M. Koch, J.W. Metzger, and J.H. Werner, submitted to Jap. J. Appl. Phys. (2016).  
 [2] R. Zapf-Gottwick, M. Koch, K. Fischer, F. Schwerdt, L. Hamann, M. Kranert, J.W. Metzger, and J.H. Werner, Int. J. Adv. Appl. Phys. Res. **2**, 7 (2015).

# Illumination Changes Leaching of Photovoltaic Modules

Simon Huber

In collaboration with: Jessica Nover,  
Renate Zapf-Gottwick, Carolin Feifel<sup>1</sup>, Michael Koch<sup>1</sup>,  
and Jürgen Werner

<sup>1</sup>Institute for Sanitary Engineering, Water Quality, and Solid Waste Management, University of Stuttgart, Germany

Leaching of hazardous and toxic substances out of photovoltaic (PV) modules is a topic of great interest. If modules are dumped or landfilled, they will remain there for a long time. For this reason, it is important to have sound knowledge about long term leaching behavior. Up to now, there were no results considering the influence of illumination on the long term leaching of PV modules.

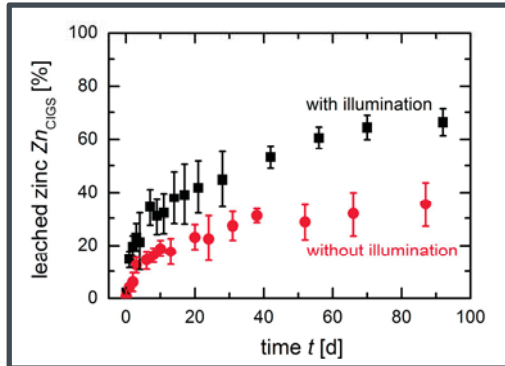
We perform leaching experiments in aqueous solutions of three different pH on 5x5 cm<sup>2</sup> module pieces, cut out from the four major PV modules: (i) crystalline silicon (c-Si), (ii) amorphous silicon (a-Si), (iii) cadmium telluride (CdTe), and (iv) copper indium gallium diselenide (CIGS). The leaching occurs at a temperature  $T = 40$  °C with agitation. A sun simulator illuminates with an irradiance  $P_{\text{opt}} = 1000$  Wm<sup>-2</sup>. The three different leaching solutions simulate the environmental conditions of acidic rain (pH3), groundwater (pH7) and alkaline landfills (pH11).

Inductively coupled plasma mass spectrometry (ICP-MS) measures the amount of eluted elements according to ISO 17294-2 [3]. We investigate: silver (Ag), aluminum (Al), cadmium (Cd), copper (Cu), gallium (Ga), indium (In), molybdenum (Mo), nickel (Ni), lead (Pb), selenium (Se), tin (Sn), tellurium (Te), and zinc (Zn).

All leaching data are given with respect to the total mass in one module piece. To determine the total mass by ICP-MS, we mill the module piece to powder, digest it with nitric acid and hydrogen peroxide, and use microwave irradiation.

Under illumination, we observe a higher leaching for the elements Cd, In, Mo, Se, Te, Zn. In contrast, Sn shows less leaching under illumination. As an example, figure 1 shows the leached amount of zinc  $Zn_{\text{CIGS}}$  out of the front contact of CIGS module pieces with and without illumination.

**Figure 1:** Leached amount of zinc  $Zn_{\text{CIGS}}$  from CIGS module pieces in pH3 solution. With illumination,  $Zn_{\text{CIGS}}$  is approximately twice as much as without illumination.



Illumination changes the leaching of the PV module pieces. Some elements show substantial higher leaching mainly within the first few days only. We suppose that the effect of illumination is caused by the voltage induced in the solar cells. With progressing elution, the cells are more and more damaged and the voltage drops. Considering this effect, elution rates under illumination are higher in the beginning and become lower when leaching proceeds.

Currently, we are developing a model, which includes thermo-dynamic properties, redox potential, pH value, and the illumination induced voltage. This model will help to qualitatively understand the exact leaching mechanisms.

**References:**

- [1] K. Huang, G. Zhuang, C. Xu, Y. Wang, and A. Tang, *Atmos. Res.* **89**, 146 (2008).
- [2] A. Dellantonio, W. Fitz, H. Custovic, F. Repmann, B. Schneider, H. Grünewald, V. Gruber, Z. Zgorelec, N. Zerem, C. Carter, M. Markovic, M. Puschenreiter, and W. Wenzel, *Environ. Pollut.* **153**, 677 (2008).
- [3] ISO 17294-2: *Water quality - Application of inductively coupled plasma mass spectrometry (ICP-MS) - Part 2: Determination of 62 elements* (2003).

# Fineline- and Double-Printing on Selective Emitter

Sabrina Lang

In collaboration with: Sabine Schreiber and  
Renate Zapf-Gottwick

The metallization of industrial solar cells is mostly based on screen printing of pastes containing silver or aluminum. For interconnecting the cells in a module by soldering, the front contacts form a grid of small fingers and busbars. This front metallization shadows part of the incoming radiation and causes optical losses [1]. To reduce these losses, the area of the front grid should be as small as possible compared to the area of the cell. In current manufacturing, the grid area takes approx. 8% of the cell with around 90 fingers of width  $60 \mu\text{m} < w_F < 70 \mu\text{m}$  and height  $h_F = 15 \mu\text{m}$ . New printing technologies and silver pastes enable the reduction of the finger width to  $w_F = 30 \mu\text{m}$ . However, printing of  $30 \mu\text{m}$  fingers suffers from a small finger height. A low resistivity of the fingers requires an aspect ratio  $a = h_F/w_F \geq 0.5$ . The necessary height  $h_F$  can not be achieved with a single printing step. Therefore, we use double-printing of the fingers ensuring a sufficient finger height. The first printing step includes the grid with the desired finger width, the second printing step uses 20% smaller fingers. The second print has to be placed exactly on top of the first print. Therefore, a precise alignment of the two printing steps is critical.

To ensure an exact positioning of the second print on top of the first print, a new screen printer together with a connected upstream adjustment unit called SAS (both from the company ASYS) was acquired. The SAS controls the positioning of the wafer in the screen printer by an AOI-system (automated optical inspection) with four cameras. Every camera takes a picture from the area in each corner of the wafer. The fingers in the recorded pictures appear brighter, than the background of the wafer. Based on this brightness difference, the AOI is able to recognize the first-print-structure. The SAS sends this information about

the position of the structure to the screen printer, thus the wafer can be aligned for the second printing step.

In cooperation with ASYS, we investigate the SAS adjustment unit with different light sources to improve the quality of the AOI-measurement. We test the illumination with four different LEDs to identify the first-print-structure. The tested LEDs are white-LED, red-LED (wavelength  $\lambda = 627$  nm), UV-LED ( $\lambda = 365$  nm) and NIR-LED (near infra-red,  $\lambda = 1550$  nm, recorded with special NIR-cameras). Unfortunately, white- and NIR-LEDs are found to be inappropriate.

Figures 1a,b show the results using the UV- and red-LED illumination. Figure 1 a) shows the insufficient performance of the UV-LED, only six measurement points are recognized by the AOI-system. Figure 1 b) shows the excellent performance of the red-LED illumination, all contact fingers are detected with good quality.

In the next step, we will examine the accuracy of the first-print-structure for double printing, before we will establish fineline- and double-printing. In further research the impact of finger-interruptions (especially the numbers and position of interruptions) on the efficiency  $\eta$  of the cell will be examined.

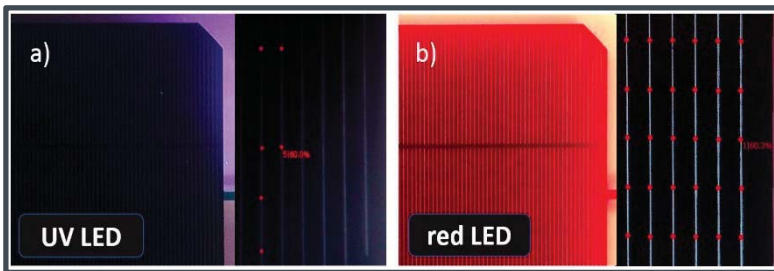


**Figure 1:** a) Recognition of the contact fingers of the first-print-structure: a) illuminated with UV-LED. The measurement is not satisfactory because only six measurement points are detected by the AOI (automated optical inspection). b) illumination with red-LED results in an excellent measurement. All possible measurement points are detected by the AOI.

#### Reference:

- [1] G. Kulushich Verlag Dr. Hut, München, Deutschland, ISBN-9783-8439-1878-7 (2014).

## Publikationen Publications

### **Silicon thin film photodetectors for multi-channel fluorescence detection in a microfluidic point-of-care testing device**

M. Berner, R. Rothemund, S. Vollmer, M.B. Schubert, U. Hilbig, and G. Gauglitz, *Phys. Status Solidi A*, 1862-6319 (2016); DOI: 10.1002/pssa.201532953

### **Amorphous Silicon Passivation for p++ and n++ Areas on IBC Solar Cells**

K. Carstens, M. Dahlinger, E. Hoffmann, J.R. Köhler, R. Zapf-Gottwick, and J.H. Werner, in *Proc. of the 4<sup>th</sup> International Education Forum on Environment and Energy Science* (2015); DOI: 10.13140/RG.2.2.13666.94407

### **Universal Passivation for p++ and n++ Areas on IBC Solar Cells**

K. Carstens, M. Dahlinger, E. Hoffmann, J.R. Köhler, R. Zapf-Gottwick, and J.H. Werner, *Energy Procedia* **77**, 779 (2015); <http://dx.doi.org/10.1016/j.egypro.2015.07.110>

### **Surface passivation of heavily boron or phosphorus doped crystalline silicon utilizing amorphous silicon**

K. Carstens, and M. Dahlinger, *J. Appl. Phys.* **119** (18), 185303 (2016); DOI: <http://dx.doi.org/10.1063/1.4948945>

### **Laser-Doped Back-Contact Solar Cells**

M. Dahlinger, B. Bazer-Bachi, T.C. Röder, J.R. Köhler, R. Zapf-Gottwick, and J.H. Werner, *IEEE J. Photovoltaics* **5**, 812 (2015).

### **23.2% Efficiency with Laser Processed IBC Solar Cells**

M. Dahlinger, K. Carstens, E. Hoffmann, S. Wansleben, J.R. Köhler, R. Zapf-Gottwick, and J.H. Werner, in *Proc. 31<sup>st</sup> Europ. Photovolt. Solar Energy Conf.*, (WIP, München, 2015), p. 462, DOI: 10.4229/EUPVSEC20152015-2DO.2.4

**Laser Processed Silicon Back Contact Solar Cells Exceeding 23% Efficiency**

M. Dahlinger, K. Carstens, E. Hoffmann, R. Zapf-Gottwick, and J.H. Werner, *in Proc. of the 4<sup>th</sup> International Education Forum on Environment and Energy Science* (2015), DOI: 10.13140/RG.2.2.26149.91365

**23.2% laser processed back contact solar cell: Fabrication, characterization and modeling**

M. Dahlinger, K. Carstens, E. Hoffmann, R. Zapf-Gottwick, and J.H. Werner, *Prog. Photovolt: Res. Appl.* **25**, 192 (2016).

**Band gap narrowing models tested on low recombination phosphorus laser doped silicon**

M. Dahlinger, and K. Carstens, *J. Appl. Phys.* **120**, 155701 (2016).

**Optimized Laser Doped Back Surface Field for IBC Solar Cells**

M. Dahlinger and K. Carstens, *Energy Procedia* **92**, 450 (2016).

**Silberreduktion in der Photovoltaik**

L. Hamann, Verlag Dr. Hut, München, Deutschland, ISBN 978-3-8439-2379-9, (2015)

**Selbstdotierende Laser-transferierte Kontakte für Silizium-solarzellen**

E. Hoffmann, Verlag Dr. Hut, München, Deutschland, ISBN 978-3-8439-2472-6, (2016)

**5" Laser-IBC Solar Cells with 22.0% Efficiency**

E. Hoffmann, M. Dahlinger, K. Carstens, S. Wansleben, R. Zapf-Gottwick, and J.H. Werner, *in Proc. 32<sup>nd</sup> Euro. Photovolt. Solar Energy Conf.*, edited by M. Topic, N. Taylor and P. Helm (WIP, Munic, 2016), p. 580; DOI: 10.4229/EUPVSEC20162016-2DO.16.5

**Enhanced Leaching of Photovoltaic Modules by Illumination**

S. Huber, J. Nover, R. Zapf-Gottwick, C. Feifel, M. Koch, J.W. Metzger, and J.H. Werner, in *Proc. of the 5<sup>th</sup> International Education Forum on Environment and Energy Science* (2016); DOI: 10.13140/RG.2.2.16293.29923

**Phosphorus out-diffusion in laser molten silicon**

J.R. Köhler, and S.J. Eisele, *J. Appl. Phys.* **117**, 145701 (2015); DOI: 10.1063/1.4917048

**The Electricity Bank: Innovative operating model for local energy storage**

T. Kropp, J. Wang, M.B. Schubert, and J.H. Werner, in *Proc. of the 5<sup>th</sup> International Education Forum on Environment and Energy Science* (2016); DOI: 10.13140/RG.2.2.11150.36162

**Infrared backwards laser melting of a silicon wafer**

P.C. Lill, and J.R. Köhler, *Eur. Phys. J. Appl. Phys.* **72**, 2 (2015); DOI: 10.1051/epjap/2015150248

**Boron Partitioning Coefficient above Unity in Laser Crystallized Silicon**

P.C. Lill, M. Dahlinger, and J.R. Köhler, *submitted to: Materials*, (2016)

**Analysis of photovoltaic system performance time series: Seasonality and performance loss**

A.Phinikarides, G. Makrides, B. Zinßer, M. B. Schubert and G. E. Georghiou, *Renew Energ* **77**, 51-63 (2015); DOI: 10.1016/j.renene.2014.11.091

**Porous Silicon Thin Film Anodes for Lithium Ion Batteries**

C. Sämann, K. Kelesiadou, S.S. Hosseinioun, M. Wachtler, J.R. Köhler, P. Birke, M. Schubert, and J.H. Werner, in *Proc. of the 5<sup>th</sup> International Education Forum on Environment and Energy Science* (2016); DOI: 10.13140/RG.2.2.35267.60962

**Pulsed laser porosification of silicon thin films**

C. Sämann, J.R. Köhler, M. Dahlinger, M.B. Schubert, and J.H. Werner, *Materials* **9**, 509 (2016); DOI: 10.3390/ma9070509

**Reversible capacity fade in lithium-ion cells at low temperatures**

J.P. Singer, and K.P. Birke, in *Proc. of the 5<sup>th</sup> International Education Forum on Environment and Energy Science* (2016); DOI: 10.13140/RG.2.2.15244.72326

**Leaching Hazardous Substances out of Photovoltaic Modules**

R. Zapf-Gottwick, M. Koch, K. Fischer, F. Schwerdt, L. Hamann, M. Kranert, J. Metzger, and J.H. Werner, *Int. j. adv. appl. phys. res.* **2**, 7, (2015); DOI: 10.15379/2408-977X.2015.02.02.2



# Lehrveranstaltungen Lectures



**Mikroelektronik I**  
**(Bachelor, Wintersemester)**

*J.H. Werner*

- Energiebänder und Leitfähigkeit
- Silizium - der Werkstoff der Mikroelektronik
- Elektronen und Löcher in Halbleitern
- Ströme in Halbleitern
- Nichtgleichgewicht, Injektion, Extraktion
- Elektrostatik des pn-Übergangs
- Ströme im pn-Übergang

**Einführung in die Elektrotechnik für Kybernetik und  
Verkehrsingenieurwesen**  
**(Bachelor, Sommersemester)**

*K.P. Birke*

- Elektrischer Gleichstrom
- Wechselstrom
- Elektrische und magnetische Felder

**Photovoltaik I**  
**(Bachelor, Sommersemester)**

*J.H. Werner*

- Der Photovoltaische Effekt: Solarzelle, -modul, -anlage
- Sonnenspektrum und -leistung,  
Energieverbrauch in Deutschland
- Maximaler Wirkungsgrad von Solarzellen
- Ersatzschaltbilder
- Photovoltaik-Materialien und -Technologien
- Modultechnik
- Photovoltaische Systemtechnik

**Optoelectronic Devices and Circuits I  
(Bachelor, Sommersemester)**

*J.H. Werner*

- Basic physics, thermal radiation
- Coherence
- Semiconductor basics
- Excitation and recombination processes
- Light emitting diodes
- Semiconductor lasers
- Glass fibers
- Photodetectors

**Laser and Light Sources  
(Master, Wintersemester)**

*J.H. Werner and J.R. Köhler*

- The Human Eye
- Light and Color
- Photometry
- Incoherent Light Sources
- Light Emitting Diodes
- Lasers
- Laser Processing

**Photovoltaik III  
(Master, Sommersemester)**

*J.H. Werner*

- Technologie einkristalliner Zellen
- Rekombinationsmechanismen
- Theorie der maximalen Wirkungsgrade
- Optimierungsstrategien
- Zweite und Dritte Generation Photovoltaik

**Battery Modelling and Energy Management  
(Master Infotech, Wintersemester)**

*K.P. Birke*

- Electrical battery models
- Aging effects in batteries
- Thermal battery models
- Implementation of battery models
- Energy management
- Sustainable energy chains
- Future concepts for battery modelling and energy management

**Energiewandlung  
(Master, Sommersemester)**

*J.H. Werner*

- Thermodynamik
- Direkte Nutzung der Sonnenenergie (Solarthermie, Photovoltaik)
- Indirekte Nutzung der Sonnenenergie (Wasserkraft, Windenergie)
- Chemische Wandlung und Speicherung elektrischer Energie (Batterien, Brennstoffzellen)

**Photovoltaik II  
(Master, Wintersemester)**

*J.H. Werner*

- Solarstrahlung
- Alternativen zu konventionellen Siliziumzellen
- Komponenten von Photovoltaikanlagen
- Planung, Installation, Betrieb und Monitoring von Photovoltaikanlagen
- Photovoltaische Messtechnik
- Markt und Wirtschaftlichkeit der Photovoltaik

### **Werkstoffe der Elektrotechnik (Master, Wintersemester)**

*K.P. Birke*

- Allgemeine Übersicht über Werkstoffe der Elektrotechnik, ihre Eigenschaften sowie Methoden der Unterteilung in verschiedene Werkstoffklassen
- Herleitung makroskopischer Eigenschaften aus dem atomaren und mikroskopischen Aufbau
- Berechnungsverfahren, Kenngrößen
- Herstellungsverfahren
- Anwendungsgebiete

### **Speichertechnik für elektrische Energie II (Master/Bachelor, Wintersemester)**

*K.P. Birke*

- Vertieftes Verständnis der mikroskopischen Abläufe in elektrochemischen Energiespeichern
- Messverfahren von ausgewählten Batterieparametern
- Elektrische Speichertechniken zur nachhaltigen elektrischen Energieversorgung
- Auslegungsverfahren für elektrische Energiespeicher in unterschiedlichen aktuellen und zukünftigen Anwendungsgebieten

### **Mobile Energiespeicher (Master/Bachelor, Wintersemester)**

*K.P. Birke*

- Anforderungen
- Aufbau
- Architekturen
- Auslegung mobiler Energiespeicher
- Einfache Berechnungsverfahren von Batteriegrößen
- Einführung in das Batteriemangement für automotiv Energiespeicher

**Wissenschaftliches Vortragen und Schreiben I  
(Master/Bachelor, Wintersemester)**

*J.H. Werner*

- Kernbotschaften
- Aufbau eines Vortrags
- Standardfehler (Strukturfehler, Technikfehler, Fehler im Auftreten)
- Praktische Schritte zum Vortrag
- Präsentation eines wissenschaftlichen Vortrages von 12 min. (mit Videoaufzeichnung)
- Selbst- und Fremdbeurteilung

**Wissenschaftliches Vortragen und Schreiben II  
(Master/Bachelor, Sommersemester)**

*J.H. Werner*

- Kernbotschaften
- Aufbau und Elemente einer Publikation
- Bilder, Tabellen, Gleichungen und Referenzen
- Verfassen eines eigenen wissenschaftlichen Kurzberichts von 4 bis 6 Seiten

**Speichertechnik für elektrische Energie I  
(Master/Bachelor, Sommersemester)**

*K.P. Birke*

- Aufbau und Funktionsweise von elektrischen Energiespeichersystemen
- Beschreibung der Speicher anhand charakteristischer Größen
- Überblick über die wichtigsten Messverfahren
- Einführung in Ersatzschaltbilder und Modellierung

**Photovoltaische Inselsysteme  
(Master/Bachelor, Wintersemester)**

*B. Zinßer*

- Typen von Inselsystemen
- Komponenten
- Auslegung
- Simulation
- Praxis
- Wirtschaftlichkeit

**Teamarbeit *ipv*  
(Bachelor, Sommersemester)**

*J.R. Köhler*

- Herstellung eines Moduls aus einkristallinen Mini-Solarzellen
- Konfigurieren eines Solarladereglers und Speicherakkus
- Charakterisierung Minimodul und Solarladeregler

**Praktische Übungen im Labor „Photovoltaik“  
(Bachelor, Sommersemester)**

*R. Zapf-Gottwick*

- Herstellung von industriellen, kristallinen Si-Solarzellen
- Messung und Auswertung der IV-Kennlinie
- Quanteneffizienz und Reflexionsmessung
- PV-Modulherstellung mit kristallinen Si-Solarzellen

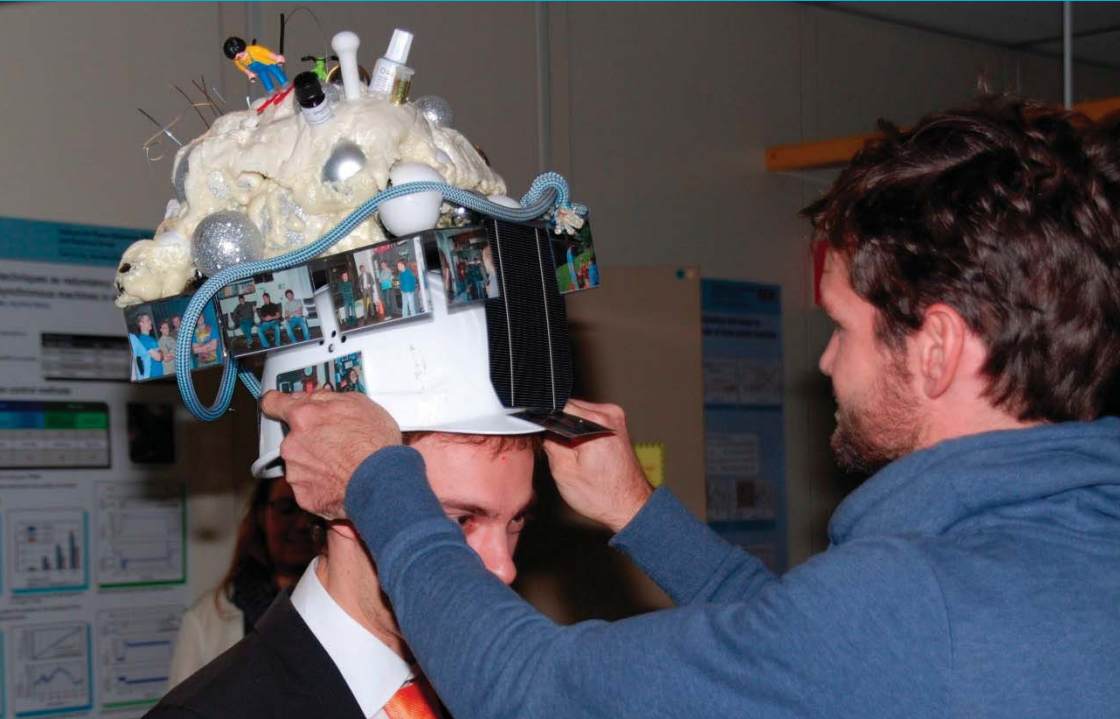
**Praktische Übungen im Labor  
„Messtechnik für Energiewandler und -speicher“  
(Master, Wintersemester)**

*R. Zapf-Gottwick und J.R. Köhler*

- Herstellung von Passivierschichten
- Charakterisierung der Schichten: Reflexion und Ellipsometrie
- Charakterisierung der Passivierschichten: Lebensdauermessungen mit PL und QSSPC
- Elektrische Charakterisierung von elektrochemischen Zellen
- Elektrochemische Charakterisierung
- Aufbau einer Li-Ionen Pouch-Zelle



# Abschlüsse Degrees



## Promotionen PhD Theses



**Lars Hamann**  
Silberreduktion  
in der Photovoltaik



**Erik Hoffmann**  
Selbstdotierende Laser-transferierte  
Kontakte für Siliziumsolarzellen

## Bachelorarbeiten Bachelor Theses

### **Yasin Atas**

Teststand für Photovoltaikmodule

### **Sebastian Bartels**

Herstellung von Strukturelementen für Li-Ionen-Zellen mit dem 3D-Drucker

### **Sebastian Bil**

Charakterisierung von negativen Elektroden für Lithium-basierte Hochenergiezellen

### **Lukas Büchner**

Jahresenergieerträge von PV-Anlagen mit Laser-Rückseitenkontakt solarzellen

### **Rafael Conradt**

Auslegung und energetische Betrachtung von Peltier-Elementen zur thermischen Regulierung von Lithium-Ionen-Akkumulatoren

### **Zübeyr Cosgun**

Langzeitdegradation von Photovoltaikmodulen

### **Christian Dias Grauer**

Aufbau einer Alkali-Mangan-Zelle mit Nickelschaum als Ableit-elektrode

### **Philipp Dress**

Untersuchung von Kohlenstoffbeschichtungen auf Nickelschäumen für den Einsatz in elektrischen Energiespeichern

### **Julian Egle**

Erstellung und Umsetzung eines PV-Laderegelungskonzepts für Luftschiffe

### **Richard Fichte**

Elektrotechnisches Balancing von Lithium-Ionen-Zellen

### **Dennis Gerber**

Auslegung und Konstruktion eines alkalischen Elektrolyseurs

**Tobias Gössl**

Optisches Simulationsmodell eines Mikrofluidikkanals für bioanalytische Fluoreszenzmessungen

**Marvin Haag**

Untersuchung der Aufspaltung von CO<sub>2</sub> über ein Plasma-verfahren und einen Festkörper-Hochtemperatur-Elektrolyseur

**Jacob Hampel**

Entwicklung eines Modems zur Powerline-Kommunikation in Automotive-Batteriesystemen

**Anya Heider**

Characterisation of an Organic-Inorganic Perovskite Material and Its Application to Solar Cells

**Julian Heydgen**

Separator mit besonderen Strukturelementen für Lithium-Zellen

**Friederike Huber**

Einfluss von Alkali-Metallen auf Kesterit-Solarzellen

**Pascal Hug**

Auswahl und Charakterisierung von Lithium-Ionen-Zellen für den Modulaufbau von selbsttragenden und leichten Einheiten

**Clemens Jurgschat**

3D-Druck von Lithium-Ionen-Batterien mit horizontalen Verbindungen

**Tijen Karimani**

Feuchtigkeitsmessung in EVA-laminierten Schichten

**Katerina Kelesiadou**

Laserinduzierte Porositätsvariation von Siliziumanoden in Lithium-Ionen-Batterien

**Mike Kopp**

Konzeption und Aufbau eines Messplatzes zur lokalen Druckbestimmung an Lithium-Ionen-Zellen

**Simon Kostelecky**

Energiebedarf eines Foodsharing-Kühlschranks

**Matthias Kraft**

Delamination von PV-Modulen durch Lösen von Rückseiten-Metallkontakten

**Maximilian Kraft**

Flexibles Solarmodul zur photovoltaischen Stromversorgung eines Luftschiffs

**Daniel Krüger**

Solarzellen im Magnetfeld

**Thomas Reinhart**

Laserstrukturierung von Aluminium für Rückseitenkontaktsolarzellen

**Jacob v. Römer**

Ablation von Passivierschichten auf Rückseitenkontaktsolarzellen

**Shima Sasanpour**

Metalloxid Oberflächenbeschichtungen für Siliziumanoden in Lithium-Ionen-Batterien

**Tobias Schmidt**

Untersuchung von Netz-kontaktierten  $\text{TiO}_2$ -Elektroden für Li-Ionen Zellen mit elektrochemischen und optischen Methoden

**Eugen Schwarzkopf**

Entwicklung eines Messchucks für 5-Zoll und 6-Zoll Rückkontaktsolarzellen

**Dominik Steller**

Zweilagige Aluminiummetallisierung durch Laserschweißen für Rückseitenkontaktsolarzellen

**Gernot Tuschewitzki**

Drone Ready DaySy

**Johannes Wanner**

Erweiterung eines Versuchsaufbaus zur Untersuchung einer plasmabasierten CO<sub>2</sub>-Zerlegung

**German Wiesel**

Entwicklung und Parametrierung eines thermischen Modells für eine Lithium-Ionen Zelle

**Fabian Winter**

Evaluierung und Optimierung der DaySy-Messmethodik

**Matthias Zorn**

Löslichkeit von Cadmiumtellurid

## Forschungsarbeiten Research Theses

### **Kayvan Azari**

Evaluierung der Bilderzeugungsalgorithmen für die DaySy Tageslichtlumineszenz

### **Lukas Billinger**

Erstellung einer Auswertungssoftware für Bilder von Photovoltaikanlagen

### **Tim Buchali**

Entwicklung von Ein- und Ausschaltstrategien für Hochvolt-Lithium-Ionen-Akkumulatoren mit Einzelzellschaltertopologie

### **Lei Chen**

Investigations on the Operation of the Strombank

### **Simon Fleischer**

Spannungsbetriebsfenster einer Lambdasonde abhängig von der Temperatur

### **Tobias Gössl**

Zyklisierbarkeit von Lithium-Metall-Elektroden bei Verwendung unterschiedlicher Elektrolyte

### **Sema Gülerüç**

Stickstoff-gesputtertes Lithiumphosphat als künstliche Deckschicht

### **Fabian Heim**

Untersuchung der Zyklisierbarkeit von Lithium-Metall-Elektroden

### **Fabian Höderath**

Konstruktion einer Elektrolytrückführung für einen alkalischen Elektrolyseur und Ermittlung der charakteristischen Zellkennlinien

### **Pascal Kölblin**

Parameter der Bildqualität zur Optimierung der Elektrolumineszenzmessung im Feld

**Martin Kynast**

Modulkonzeption/-konstruktion von selbsttragenden und leichten Einheiten aus Li-Ionen-Zellen

**Ioannis Lambidis**

Projekt Strombank – Datenanalyse der ersten Messwerte aus der Praxis

**Alexander Möller**

Messaufbau zur Bestimmung von Kleinsignaldetektionsgrenzen von Dünnschichtphotodioden

**Daniel Müller**

Optimierung des Ladeprofils einer EV-Flotte im Rahmen einer Micro Smart Grid Simulation

**Patrick Pascher**

Entwicklung eines parametrischen Modells zur thermischen Modellierung eines Batteriemoduls aus Lithium-Ionen-Zellen

**Hannes Schneider**

Experimental Parameter Estimation for a High Frequency Battery Model and Analysing Its Operation in Connection with a DC/DC Converter

**Thomas Schuster**

Wasserstoffherzeugung mittels Umsetzung von Metallen, Halbmetallen und Halbleitern

**Christian Seidler**

Entwicklung und Implementierung einer Methode zur Ladezustandserkennung von Li-Ionen-Zellen

**Marcel Waldhof**

Graphical User Interface – Annotierung und statistische Auswertung von Messbildern mit Matlab

**Juncheng Wang**

Supply of Balancing Energy by the Strombank

**Felix Wenzler**

Entwicklung von Lehrinhalten zu erneuerbaren Energien in ländlichen Regionen Indonesiens und deren praktische Anwendung

**Yi Yi**

DC-Netze in Nichtwohngebäuden

**Ruyin Zhang**

Materialcharakterisierung von n-Typ Wafern

**Matthias Zorn**

Druckkontaktierte Zellverbinder für Li-Ionen-Rundzellen

## Masterarbeiten Master Theses

**Markus Botey-Junca**

Oberflächenbearbeitung von Metallen durch Laserlegieren

**Ludwig Eringer**

Aufbau und Modellierung einer Energiespeichereinheit mit unterschiedlichen elektrochemischen Zellen

**Anja Heinzlmann**

Infrarot Laserporosieren von Dünnschichtsilizium als Anode in Lithium-Ionen-Akkumulatoren

**Simon Huber**

Messplatzaufbau: Elektrochemisches Auslaugen von PV-Modulstücken unter Beleuchtung

**Terpsithea Karadali**

Synthese und Modifikation sauerstoffhaltiger Elektrodenmaterialien für Lithium-Ionen-Zellen durch elektromagnetische Strahlung

**Sascha Koch**

Machbarkeitsnachweis des Fourier Transform Imagers

**Martin Kynast**

Konzeption und Konstruktion zweier Batteriemodule mit Rund- und Pouchzellen und Vergleiche der wichtigsten KPIs

**Ioannis Lambidis**

Aufbau und Lademanagement einer Energiespeichereinheit mit unterschiedlichen elektrochemischen Zellen

**Alexander Möller**

Aufbau und Implementierung eines optisch entkoppelten Batteriemanagementsystems

**Daniel Müller**

Plasmabasierte Methanisierung von Kohlendioxid mit zusätzlichem Sauerstoff-Ionenleiter

**Thomas Nauhauser**

Entwicklung einer passiven Impedanzmessmethode für Akkumulatoren

**Andre Pfeiffer**

Entwicklung und Aufbau einer Batteriemangement-Workbench

**Fabian Puntigam**

Entwicklung eines Messsystems zur parallelen, synchronen Kennlinienmessung räumlich verteilter Solarzellen

**Aref Samadi**

Implementation and Characterization of an IV Measurement Setup for Interdigitated Back Contact Solar Cells

**Bernd Schrettle**

Aufbau und Inbetriebnahme eines Messplatzes für elektrochemische Zellen

**Ismail Shokry**

Bifacial Modules – Simulation and Experiment

**Juncheng Wang**

Scaled Simulation of a 100 kWh Lithium-Ion Battery Storage

**Yi Wang**

Development and Parameterization of Lithium-Ion-Battery Cell Models

**Felix Wenzler**

24-Stunden-Solarmodul

**Daniel Wolpert**

Potential automotiver Li-Ionen-Batterien in stationären Anwendungen

**He Yang**

Charakterisierung und Modellierung des Alterungsverhaltens von Lithium-Ionen-Batterien

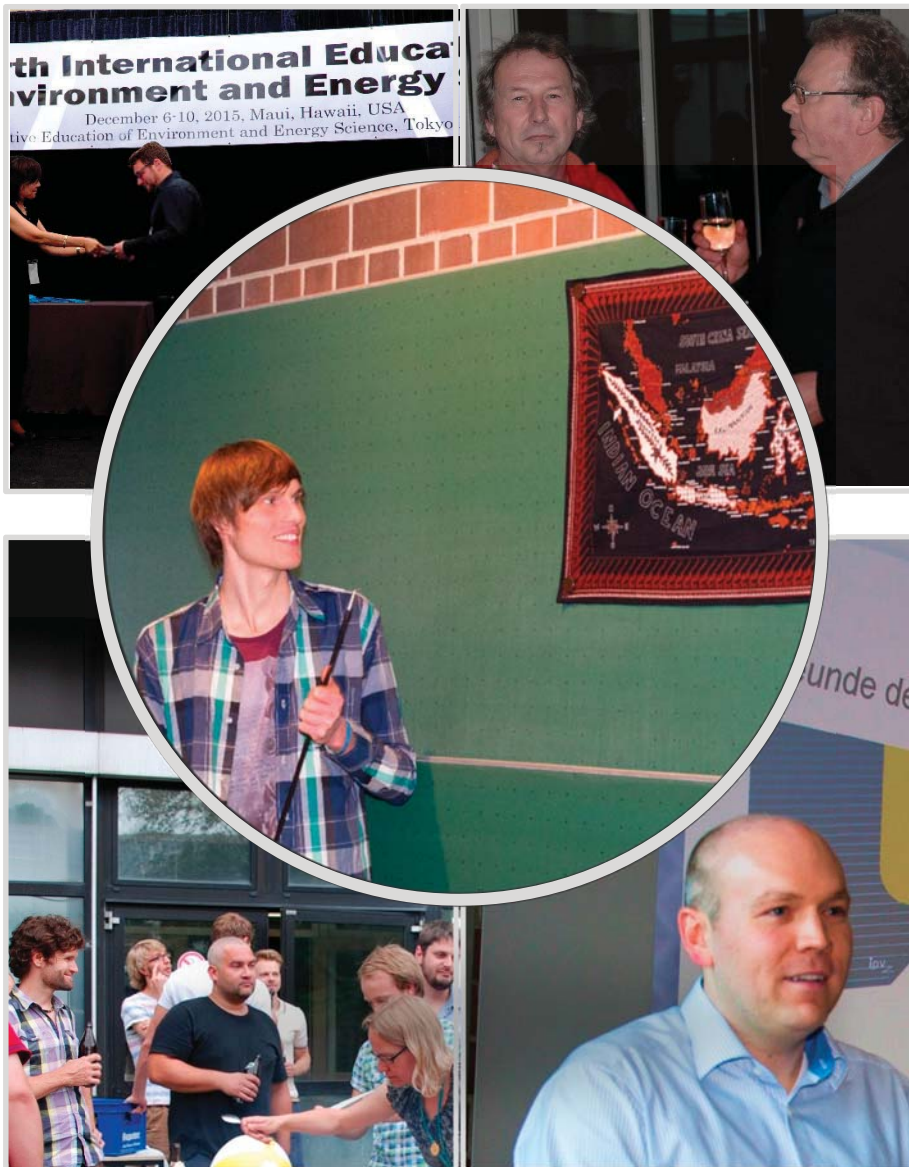
**Lea Zeiner**

Zellverbindung im Modul durch Laserschweißen

**Junying Zhao**

Runge-Kutta Solver for the Numerical Simulation of the Laser-Doping Process

# Was sonst noch war ... Beyond Science ...



#### **40-jähriges Dienstjubiläum**

Leonhard Bauer hat es geschafft! 40 Jahre seines Arbeitslebens hat er der Universität Stuttgart gewidmet. Wir hoffen alle, dass uns Leo noch möglichst lange erhalten bleibt. Herzlichen Glückwunsch, Leo!

#### **Professor Dr.-Ing. Kai Peter Birke kommt ans *ipv***

Zum 01.02.2015 wurde Kai Peter Birke ans *ipv* berufen. Er leitet unsere neue Forschungsgruppe Elektrische Energiespeichersysteme.

#### **ACEEES Forum 2015**

Beim *4<sup>th</sup> International Education Forum on Environment and Energy Science* erhielt Marcel Berner den Preis für den besten wissenschaftlichen Vortrag. Dieses Forum wird von der *Academy for Co-creative Education of Environment and Energy Science (ACEEES)* des *Tokyo Institute of Technology* veranstaltet.

---

#### **40<sup>th</sup> Anniversary**

Leonhard Bauer made it! He has dedicated 40 years of his working life to the University of Stuttgart. We all hope that Leo will stay with us for as long as possible! Congratulations, Leo!

#### **Professor Dr.-Ing. Kai Peter Birke joins the *ipv***

On February 2<sup>nd</sup> in 2015, Kai Peter Birke was appointed professor at the *ipv*. He is the head of our new research group Electrical Energy Storage Systems.

#### **ACEEES Forum 2015**

At the *4<sup>th</sup> International Education Forum on Environment and Energy Science*, Marcel Berner won the award for the best scientific presentation. This forum is organized by the *Academy for Co-creative Education of Environment and Energy Science (ACEEES)* of the *Tokyo Institute of Technology*.

### **Sommerfeste 2015 und 2016**

Auch in den letzten beiden Jahren haben wir zum Ende des Sommersemesters ein Grillfest veranstaltet, bei dem die Studenten der Vorlesung Energiewandlung die Gelegenheit nutzten, ihre Projekte und Prototypen vorzustellen.

### **ACEEES Forum 2016**

Beim *5<sup>th</sup> International Education Forum on Environment and Energy Science* erhielt Simon Huber den Preis für den besten wissenschaftlichen Vortrag.

### **Reinraumumbau**

Seit November 2015 wird der Reinraum des *ipv* umgebaut: Erneuerung aller Zu- und Abluftkanäle, neue Regelungstechnik für Abluftüberwachung. Die Kosten hierfür sind mit 975.000,- € veranschlagt. Die Arbeiten sollen bis Mitte April 2017 abgeschlossen sein.

---

### **Summer Barbecues 2015 and 2016**

At our traditional barbecues at the end of the summer terms of 2015 and 2016, the students of the lecture Energy Conversion had the opportunity to present their projects and prototypes.

### **ACEEES Forum 2016**

At the *5<sup>th</sup> International Education Forum on Environment and Energy Science*, Simon Huber obtained the award for the best scientific presentation.

### **Retrofit of the Cleanroom**

Since November 2015, the cleanroom of the *ipv* is being retrofitted: replacement of all air supply ducts and exhaust air ducts, new technology for the monitoring and control of exhaust air. Estimated costs amount to 975,000 €. The construction works are supposed to be finished by the middle of April 2017.

# Stuttgarter Photovoltaik Preise 2015/16 Photovoltaic Awards of Stuttgart 2015/16

Stuttgarter  
Photovoltaik Preis 2015



Stuttgarter  
Photovoltaik Preis 2016



### **Stuttgarter Photovoltaik Preise 2015 und 2016**

Der Förderverein der Freunde des Instituts für Photovoltaik (VF-*ipv*) hat im Januar 2016 und Februar 2017 acht herausragende studentische Arbeiten prämiert und die *Stuttgarter Photovoltaik Preise* im Rahmen eines Fest-Kolloquiums an die Studierenden verliehen.

Der gemeinnützige Förderverein VF-*ipv* unterstützt seit seiner Gründung im Juli 2010 die wissenschaftliche Forschung und Arbeit am *ipv* und fördert den wissenschaftlichen Nachwuchs.

---

#### **Die Preisträger 2015 und 2016 sind:**

**The 2015 and 2016 award winners are:**

Bachelorarbeiten/Bachelor Theses:

Tobias Gössl, Julian Egle

Projektarbeit/Project Work:

Richard Fichte, Marvin Haag, Tobias Schmidt,  
Julia Schnaars

Forschungsarbeiten/Research Theses:

Felix Wenzler, Pascal Kölblin

Masterarbeiten/Master Theses:

Anja Heinzelmann, Fabian Puntigam, Andre Pfeiffer

---

#### **Photovoltaic Awards of Stuttgart 2015 and 2016**

The association „Freunde des Instituts für Photovoltaik“ (VF-*ipv*) awarded prizes to eight excellent students theses during colloquium ceremonies in January 2016 and February 2017.

Since its foundation in 2010, the nonprofit association VF-*ipv* has supported scientific research and work at the *ipv* and encouraged young scientists.



## Mitarbeiterliste Staff Members



Gäste | Guests

Lageplan | Location Map

## Mitarbeiter Staff Members

Name	Telefon 0711- 685-...	E-Mail (vorname.name@ ipv.uni- stuttgart.de)	Arbeitsgebiet
Leo Bauer	60105	leo.bauer	Halbleiter- technologie
Lydia Beisel	67169	lydia.beisel	Halbleiter- technologie
Peter Birke	67180	peter.birke	Gruppenleiter Elektrische Energiespeicher- systeme
Christoph Bolsinger	67181	christoph. bolsinger	Elektrische Energiespeicher- systeme
Kai Carstens	67161	kai.carstens	Industrielle Solarzellen
Morris Dahlinger	67179	morris. dahlinger	Laserprozesse
Mohamed Hassan	67163	mohamed. hassan	Laserprozesse
Freyмут Hilscher	67141	freymut.hilscher	Verwaltung
Erik Hoffmann	60106	erik.hoffmann	Industrielle Solarzellen
Simon Huber	69218	simon.huber	Industrielle Solarzellen

Name	Telefon 0711- 685-...	E-Mail (vorname.name@ ipv.uni- stuttgart.de)	Arbeitsgebiet
Irmy Kerschbaum	67158	irmy. kerschbaum	Verwaltung
Jürgen Köhler	67159	juergen.koehler	Gruppenleiter Laserprozesse
Timo Kropp	67246	timo.kropp	Sensorik
Sabrina Lang	67245	sabrina.lang	Industrielle Solarzellen
Patrick Lill	67171	patrick.lill	Laserprozesse
Brigitte Lutz	67200	brigitte.lutz	Halbleiter- technologie
Hendrik Moldenhauer	67142	hendrik. moldenhauer	Halbleiter- technologie
Jessica Nover	69213	jessica.nover	Industrielle Solarzellen
Sabine Ost	67141	sabine.ost	Verwaltung
Anton Reiß	67214	anton.riss	Halbleiter- technologie
Christian Sämann	67178	christian. saemann	Sensorik

Name	Telefon 0711- 685-...	E-Mail (vorname.name@ ipv.uni- stuttgart.de)	Arbeitsgebiet
Alexander Schmid	69223	alexander.schmid	Elektrische Energiespeicher- systeme
Sabine Schreiber	67231	sabine.schreiber	Industrielle Solarzellen
Markus Schubert	67145	markus.schubert	Gruppenleiter Sensorik
Jan Singer	69217	jan.singer	Elektrische Energiespeicher- systeme
Friedrich Speckmann	67182	friedrich.speckmann	Elektrische Energiespeicher- systeme
Osama Tobail	69216	osama.tobail	Industrielle Solarzellen
Jürgen Werner	67140	juergen.werner	Institutsleiter
Birgitt Winter	67162	birgitt.winter	Gruppenleiterin Halbleiter- technologie
Renate Zapf- Gottwick	69225	renate.zapf- gottwick	Gruppenleiterin Industrielle Solarzellen

## Gäste & ausländische Stipendiaten Guests

### **Felipe Batista e Batistão**

UFSJ-Universidade Federal De São João Del Rei, São João Del Rei / Brasilien

### **Paulo Henrique Duarte Gonçalves**

UFSJ-Universidade Federal De São João Del Rei, São João Del Rei / Brasilien

### **Takahito Nishimura**

Tokyo Institute of Technology, Tokio / Japan

### **Worabhorn Pathanatecha**

Chulalongkorn University, Bangkok / Thailand

### **Guru Raghav Raman**

National Institute of Technology, Tiruchirappalli / Indien

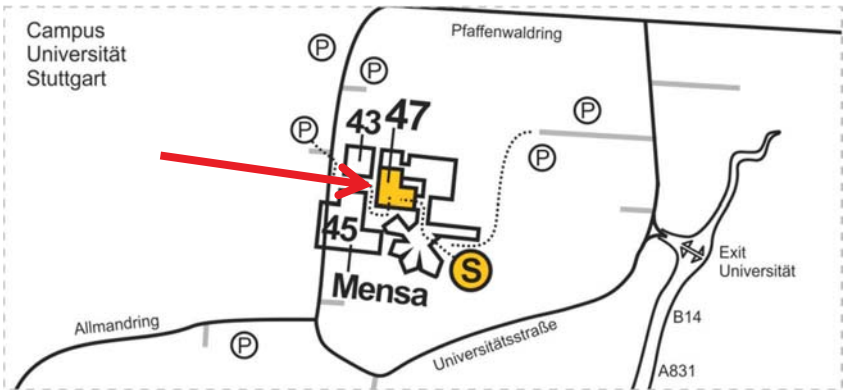
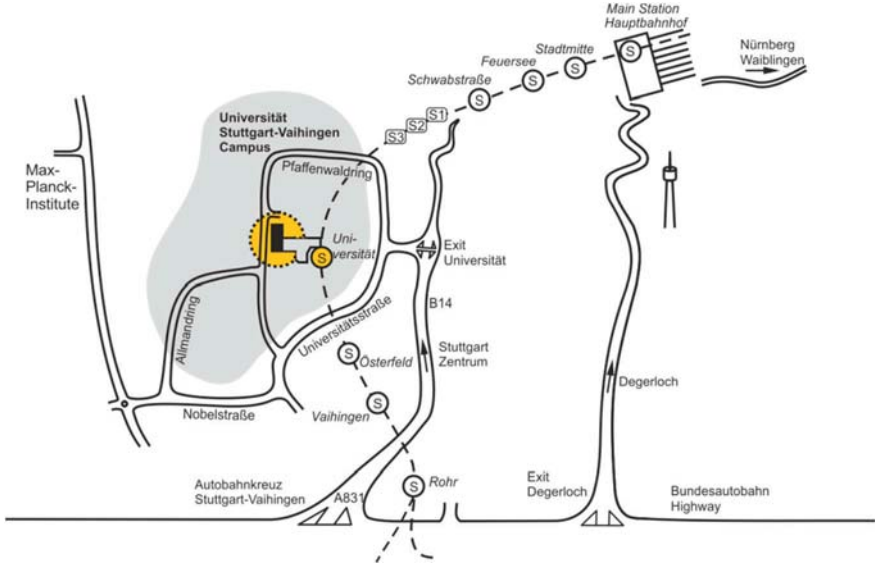
### **Kanta Sugimoto**

Tokyo Institute of Technology, Tokio / Japan

### **Dr. Khaled Ebnalwaled**

South Valley University, Qena / Ägypten

# Lageplan Location Map





**Institut für Photovoltaik  
Universität Stuttgart**

Paffenwaldring 47  
70569 Stuttgart

Phone: +49 711 685 67141

Fax: +49 711 685 67143

[www.ipv.uni-stuttgart.de](http://www.ipv.uni-stuttgart.de)

